Charles University in Prague
Faculty of Mathematics and Physics

DIPLOMA THESIS

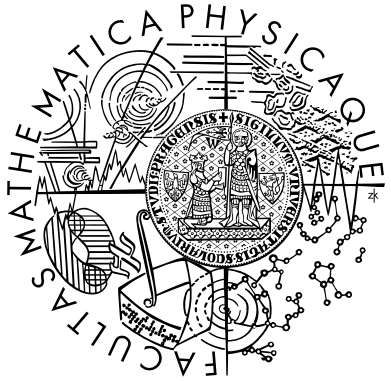

Milan Berta

Wide-range dielectric spectroscopy of relaxor type ferroelectric material $Pb(Fe_{2/3}W_{1/3})O_3$-$PbTiO_3$

Department of Dielectrics,
Institute of Physics,
Academy of Sciences of Czech Republic
Supervisor of Diploma Thesis: RNDr. Stanislav Kamba, CSc.
Study programme: Physics, Physics of Optics and Optoelectronics

Twenty to twenty-five! These are the years! Don't be content with things as the are. . . Don't take No for an answer. Never submit to failure. Do not be fobbed off with mere personal success or acceptance. You will make all kinds of mistakes; but as long as you are generous and true, and also fierce, you cannot hurt the world or even seriously distress her. She was made to be wooed and won by youth. She has lived and thrived by repeated subjugations.

Winston Churchill

I would like to express my sincere gratitude to my graduate supervisor Stanislav Kamba, for providing me the possibility to work in his group, for introducing me into the topic and last but not least for the constant support, guidance, motivation and advice; and the members of the dielectric group for the pleasant and helpful atmosphere.

Support through samples preparation by Paula M. Vilarinho (Universidade de Aveiro, Portugal) and language corrections by my colleague Ivan Gregora are also acknowledged.

I would like to thank my family for all the support they provided.

This work was supported by the Grant Agency of the Academy of Sciences of the Czech Republic, project No. A1010213.

I confess I have written my diploma thesis on my own, using only quoted sources. I agree with lending of the thesis.

Prague, 22nd April 2005 Milan Berta

Název práce: Širokopásmová dielektrická spektroskopie relaxačního ferroelektrika $Pb(Fe_{2/3}W_{1/3})O_3$-$PbTiO_3$

Autor: Milan Berta

Katedra (ústav): Oddělení dielektrik, Fyzikální ústav, AV ČR

Vedoucí diplomové práce: RNDr. Stanislav Kamba, CSc., Na Slovance 2, Praha 8

e-mail vedoucího: kamba@fzu.cz

Abstrakt: Je poskytnut úvod do základní problematiky dielektrické odezvy dielektrik, feroelektrik a relaxačních feroelektrik v okolí fázových přechodů. Tři experimentální metody (vysokofrekvenční dielektrická, časově-rozlišená terahertzová a Fourierova infračervená spektroskopie) byly použity ke studiu keramik $Pb(Fe_{2/3}W_{1/3})O_3$-$PbTiO_3$ s různou koncentrací $PbTiO_3$—0%, 25% a 37%. Měření byla prováděna při teplotách $20 - 550$ K ve frekvenčním oboru 1 MHz $- 100$ THz. Ve vysokofrekvenčních dielektrických spektrech čistého $Pb(Fe_{2/3}W_{1/3})O_3$ bylo pozorováno typické relaxorové chování, které bylo vysvětleno postupným měknutím a rozšiřováním dielektrické relaxace s ochlazováním. U $Pb(Fe_{2/3}W_{1/3})O_3$ s přídavkem 25% $PbTiO_3$ byl pozorován difůzní feroelektrický fázový přechod spojený s měknutím (nad T_c) a následným tvrdnutím (pod T_c) mikrovlnné relaxace. $Pb(Fe_{2/3}W_{1/3})O_3$ s přídavkem 37% $PbTiO_3$ vykazuje normální feroelektrický fázový přechod spojený opět s anomální mikrovlnnou relaxací. V infračervených reflexních spektrech nebyl pozorován feroelektrický měkký mód, což svědčí o fázových přechodech typu uspořádání-neuspořádání ve všech studovaných keramikách.

Klíčová slova: relaxačné ferroelektrika, ferroelektrické fázové přechody, dielektrická a infračervená spektroskopie

Title: Wide-range dielectric spectroscopy of relaxor type ferroelectric material $Pb(Fe_{2/3}W_{1/3})O_3$-$PbTiO_3$

Author: Milan Berta

Institute: Department of Dielectrics, Institute of Physics, AS CR

Supervisor: RNDr. Stanislav Kamba, CSc., Na Slovance 2, Prague 8

Supervisor's e-mail address: kamba@fzu.cz

Abstract: Basic overview of complex dielectric response of dielectrics, ferroelectrics and relaxor ferroelectrics in the vicinity of phase transitions is given. Three experimental techniques (high-frequency dielectric, time-domain terahertz and Fourier transform infrared spectroscopy) were used to study the solid solution $Pb(Fe_{2/3}W_{1/3})O_3$—$PbTiO_3$ ceramics with different $PbTiO_3$ concentrations—0%, 25% and 37%. The measurements were performed in the $20 - 550$ K temperature range and in the 1 MHz $-$ 100 THz frequency range. The typical relaxor behavior was observed in high-frequency dielectric spectra of pure $Pb(Fe_{2/3}W_{1/3})O_3$, which was explained by gradual slowing down and broadening of the dielectric relaxation on cooling. In $Pb(Fe_{2/3}W_{1/3})O_3$ with 25% $PbTiO_3$ a diffuse ferroelectric phase transition connected with a softening (above T_c) and hardening (below T_c) of microwave relaxation was observed. $Pb(Fe_{2/3}W_{1/3})O_3$ with 37% $PbTiO_3$ shows a normal ferroelectric phase transition also connected with the anomalous microwave relaxation. In infrared reflectivity spectra no ferroelectric soft mode was observed, which demonstrates the order-disorder character of phase transitions in all studied ceramics.

Keywords: relaxor ferroelectrics, ferroelectric phase transitions, dielectric and infrared spectroscopy

Table of Contents

Chapter 1

Introduction

Dielectric materials have been, in comparison with semiconductors, long time on the periphery of applied research, but the situation dramatically changed in the last ten years in view of miniaturization of integrated circuits. Replacement of mostly used SiO_2 and SiO_xN_y (as low-permittivity capacitors and gate dielectrics) with some high-permittivity materials has been required. Strict requirements are put on such new materials: higher permittivity, low leakage current, low temperature of the fabrication, good compatibility of the film with the silicon technology, low cost, etc.

Among the tested materials ferroelectrics exhibit higher permittivity than other dielectrics. Their value of permittivity can be controlled by external electric field, which can be used in advantage in tunable high-frequency devices (used in mobile communications, in microelectronic circuits as thin films). Ferroelectricity was discovered firstly in Rochelle Salt in 1920, then in KDP in 1935 and in $BaTiO_3$ in 1945 [Lines77]. The thermodynamical theory of the phase transitions had been developed by Landau in 1937 [Landau37, Landau64], further development was done by Anderson [Anderson60] and Cochran [Cochran59] in 1960. Their works showed that a lattice instability is responsible for ferroelectric phase transition, and introduced the concept of a soft mode.

Ferroelectric materials are nowadays used in a variety of applications such as high permittivity capacitors, ferroelectric memories (FRAMs), pyroelectric sen-

sors, piezoelectric transducers (buzzers, speakers), electrooptic devices (waveguide modulators, frequency doublers), etc.

In 1997 Park and Shrout published a paper [Park97] about discovery of giant piezoelectricity in solid solutions of ferroelectrics relaxors $Pb(Mg_{1/3}Nb_{2/3})O_3$ and $Pb(Zn_{1/3}Nb_{2/3})O_3$ with a ferroelectric $PbTiO_3$. This paper kicked off intensive investigation of piezoelectrics with morphotrophic phase boundary as well as of pure relaxor ferroelectrics. The glass-like, or relaxor, properties of ferroelectrics have been one of the "hot" topics in the field during the past several years [Ye98a, Vugmeister97, Cross94] (and their applications were suggested [Uchino94, Szwagierczak04]). Nowadays it is generally accepted that the strong dielectric dispersion, which occurs in relaxor ferroelectrics in a broad spectral range from terahertz to milihertz frequencies is a consequence of the dynamics of polar nanoregions, which appear several hundred degrees above T_m (temperature of permittivity maximum) at so-called Burns temperature T_d [Ye98a, Cross94]. The polar nanoregions are somehow connected with chemical and structural disorder, but there are still many open questions in the detailed description.

The aim of this manuscript is to present results of our studies obtained on solid solutions of relaxor ferroelectric $Pb(Fe_{2/3}W_{1/3})O_3$ with ferroelectric $PbTiO_3$ (PFW-PT). This system exhibits multiferroic properties (i. e., both ferroelectric and ferromagnetic), which can be used in various technical applications.

The study of the mentioned ceramics by means of high-frequency dielectric, terahertz and infrared spectroscopy is described. The techniques used were Fourier transform infrared (FT-IR) spectroscopy ($3 \times 10^{11} - 10^{14}$Hz, $10 - 3000\,cm^{-1}$) in the temperature region $20 - 550\,K$, time-domain terahertz spectroscopy (TDTS) ($10^{11} - 2.5 \times 10^{12}\,Hz$, $0.3 - 80\,cm^{-1}$) in the temperature region $20 - 300\,K$, and high-frequency (HF) dielectric spectroscopy ($10^6 - 1.8 \times 10^9\,Hz$, up to microwave range) for $100 - 500\,K$. The obtained dielectric spectra from FT-IR (far-infrared (FIR) and middle-infrared (MIR) frequency range), and HF dielectric measurements too, have been analyzed together with the experimental data from TDTS. The HF and THz measurements at different temperatures provide important information about the relaxator dynamics. The information about phonons dynamics is given by FT-IR measurements.

The manuscript is divided into three parts. The first part gives an overview of the physics in the used material (dielectric response of dielectric and ferroelectric material in a wide frequency range, ferroelectric and relaxor behavior). The second part treats the spectroscopy techniques that have been used for the measurements. Also it contains a description of data evaluation and data processing techniques, including the models of the dielectric dispersion that were applied for description of the experimental data and measurements. The third part presents the experimental data and the results obtained for various solid solutions of $Pb(Fe_{2/3}W_{1/3})O_3$ and $PbTiO_3$ (PFW-PT), and their analysis.

Chapter 2

Theoretical Concepts

2.1 Dielectric Polarization and Dielectric Function

Dielectrics are non-conducting materials with a large energy gap. Dielectrics are described by relative permittivity, ε_r, the material parameter that makes the bridge between externally applied electric field $\mathbf{E}$ and electrical polarization $\mathbf{P}$ (and dielectric displacement $\mathbf{D}$). Homogeneous electric field $\mathbf{E}$ induces homogeneous polarization $\mathbf{P}$,

$$\mathbf{P} = \varepsilon_0 \chi \mathbf{E}, \tag{2.1}$$

where ε_0 is the permittivity of vacuum, and χ is the dielectric susceptibility. Relative permittivity, ε_r, of an isotropic or cubic medium is defined by the relation

$$\varepsilon_r = \frac{\varepsilon_0 \mathbf{E} + \mathbf{P}}{\varepsilon_0 \mathbf{E}} = 1 + \chi, \tag{2.2}$$

where $\varepsilon_0 \mathbf{E} + \mathbf{P} = \mathbf{D}$ is the dielectric displacement [Waser03, Kittel85].

The dielectric function—complex permittivity, $\varepsilon^* = \varepsilon_r$, is sometimes loosely referred to as "dielectric constant" of the material. In fact it is not a constant, it depends on frequency, temperature, pressure, entropy, mechanical and electrical stresses/strains, etc., $\varepsilon^* = \varepsilon^*(f, T, p, x, \dots)$. It is a scalar variable only in the case of isotropic medium, generally it is a tensor variable represented as 3×3 matrix. Let us restrict our further discussion to one type of external field, temperature. Its variation was important in our experiments and measurements.

When time-dependent electric field is applied (let us further consider harmonic function with a constant angular frequency, ω), moving charges cause a frequency-dependent phase shift between the applied field and the charge displacement. Relative dielectric permittivity is then written as complex function,

$$\varepsilon_r(\omega) = \varepsilon^*(\omega) = \varepsilon'(\omega) - i\varepsilon''(\omega). \tag{2.3}$$

The real, ε', and imaginary, ε'', parts are connected to complex refractive index $n^* = n - i\kappa$ as follows,

$$\varepsilon'(\omega) = n^2(\omega) - \kappa^2(\omega), \qquad \varepsilon''(\omega) = 2n(\omega)\kappa(\omega), \tag{2.4}$$

where $n(\omega)$ and $\kappa(\omega)$ is the real and the imaginary part of the complex refractive index.

2.2 Frequency Dependence of the Dielectric Function

The total polarization of dielectric materials results from four contributions, as follows [Waser03, Kittel85]:

- electronic polarization (displacement of the negatively charged electron shell against the positively charged nucleus),
- ionic polarization (mutual displacement of the positive and negative sublattices under the influence of an applied electric field),
- orientational polarization (alignment of permanent dipoles), and
- space charge polarization (polarization effect in a dielectric material showing spatial inhomogeneities of charge carrier densities).

Each contribution stems from a short-range movement of charges that respond to an electric field on different time scales, hence, through a Fourier transform, in different frequency regimes. Schematic dispersion of the real and imaginary part of the dielectric function is shown in Figure 2.1. It is seen that the static permittivity, $\varepsilon'(\omega = 0)$, is determined by a sum of all polarization contributions,

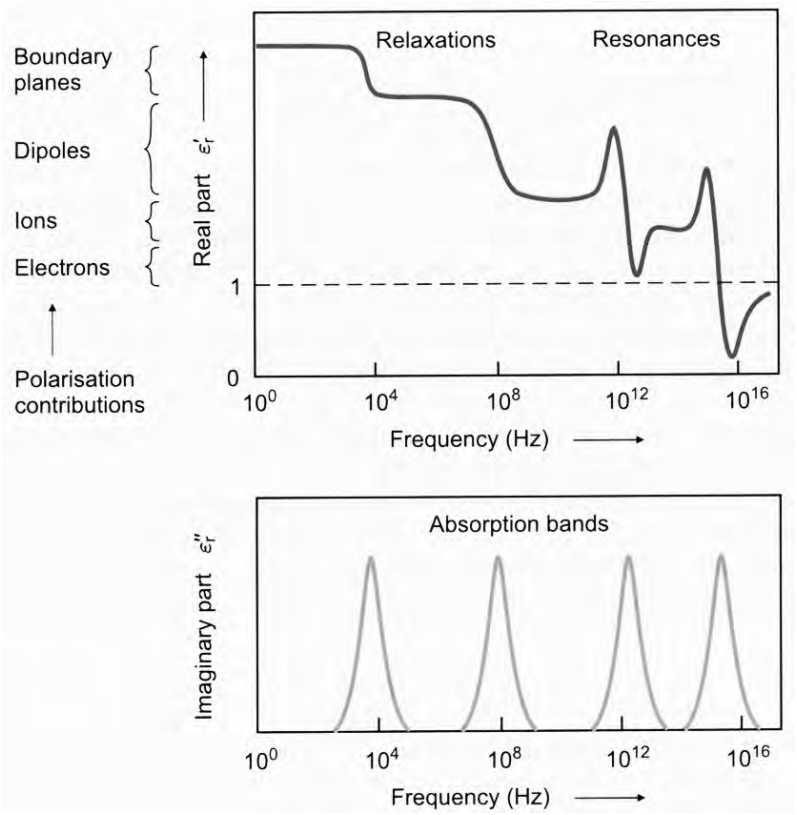

Figure 2.1 Frequency dependence of the real (top) and the imaginary (bottom) part of dielectric function [Waser03].

$\Delta\varepsilon_j'$. Each of the contributions has characteristic frequency (where maximum of dielectric loss function appears, see lower part of Figure 2.1).

The different polarization mechanisms not only take place on different time scales but also exhibit a different frequency dependence. Depending whether the oscillating masses experience a restoring force or not, we distinguish between resonance effects and relaxation effects, respectively. Resonances are observed for the ionic (molecular vibrations and ionic lattices in the infrared (IR) region, $10^{11} - 10^{13}$ Hz) and electronic polarization (above 10^{13} Hz), while relaxation effects are found for orientational polarization (electric dipoles from mHz up to GHz) and space charge polarization (from mHz up to MHz).

The whole dielectric function, ε^*, can be expressed as a sum of all polarization contributions of relaxators and oscillators:

$$\varepsilon^*(\omega) = 1 + \Delta\varepsilon_{\text{relaxators}}(\omega) + \Delta\varepsilon_{\text{phonons}}(\omega) + \Delta\varepsilon_{\text{electrons}}(\omega) =$$
$$= 1 + \sum_j \frac{\omega_{\text{r},j}\Delta\varepsilon'_j}{\omega_{\text{r},j} + \text{i}\omega} + \sum_{j_{\text{phonons}}} \frac{\Delta\varepsilon'_j\omega^2_{\text{o},j}}{\omega^2_{\text{o},j} - \omega^2 + \text{i}\omega\gamma_{\text{o},j}} + \sum_{j_{\text{electrons}}} \frac{\Delta\varepsilon'_j\omega^2_{\text{o},j}}{\omega^2_{\text{o},j} - \omega^2 + \text{i}\omega\gamma_{\text{o},j}}, \quad (2.5)$$

where variables $\omega_{\text{r},j}$ and $\gamma_{\text{r},j}$ characterize the relaxators, and $\omega_{\text{o},j}$ and $\gamma_{\text{o},j}$ the oscillators; in the latter case we distinguished the groups of oscillators composed by phonons and electrons. It holds: $1 + \Delta\varepsilon_{\text{electrons}}(\omega) = \varepsilon'_\infty$.

2.3 Ferroelectrics

Ferroelectrics are dielectrics which show a spontaneous electric polarization and in which the direction of the polarization can be reoriented between crystallographically defined states by an external electric field (hysteresis loop exists) [Waser03, Samara01].

Ferroelectric substances lose their intrinsic spontaneous polarization (their ferroelectricity) at temperature above the Curie-Weiss temperature (transition or critical temperature), T_c, and become paraelectric. Static permittivity, $\varepsilon'(0)$, follows the Curie-Weiss law above the transition temperature:

$$\varepsilon'(0) = C_{\text{CW}}(T - T_\text{c})^{-1}, \quad (2.6)$$

where C_{CW} and T_c are the Curie-Weiss constant and the Curie-Weiss temperature, respectively.

2.3.1 Perovskite Structure

From the symmetry point of view, the ferroelectrics crystallize in non-centrosymmetric space groups. Many ferroelectrics (as well as our studied system) crystallize in perovskite (ABO_3) structure. This is a large family of materials that derive their name from a $CaTiO_3$ mineral known as perovskite. The parent material,

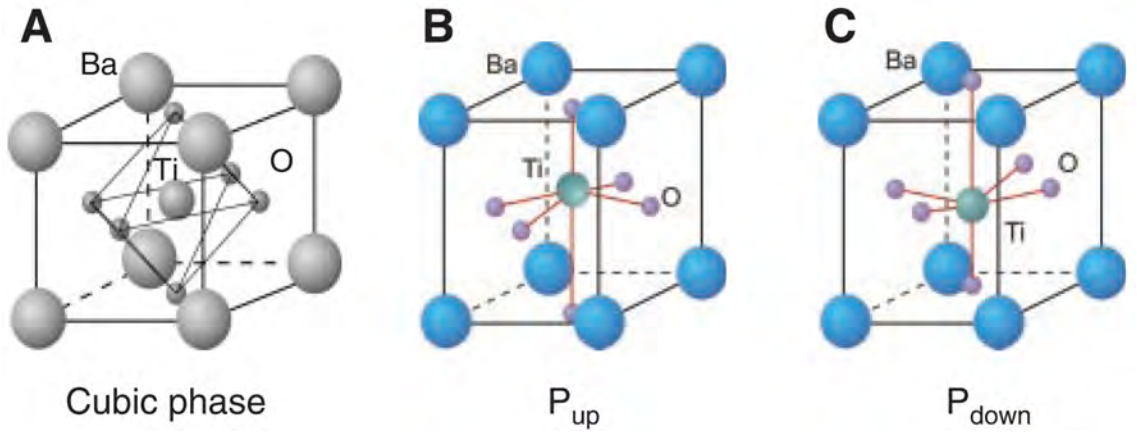

Figure 2.2 Crystal structure of the perovskite ferroelectric $BaTiO_3$. (A) High temperature, paraelectric, cubic phase. (B and C) Room temperature, ferroelectric, tetragonal phases, showing up and down polarization variants. The atomic displacements are scaled to be clearly visible [Ahn04]. Ba atoms are situated in A-sites and Ti atoms in B-sites.

perovskite, was first described in the 1830's by the geologist Gustav Rose, who named it after the Russian Count Lev Aleksevich von Perovski.

Perovskite can be thought of as a face centered cubic (FCC) lattice with A atoms at the corners and the O (oxygen) atoms on the faces as can be seen in Figure 2.2. In the paraelectric (PE) phase the B atoms sit in the center of the unit cells, in the ferroelectric (FE) phase the A and B atoms are shifted relatively to the negatively charged oxygens (see Figure 2.2), producing a polarization. This scheme is valid only in the case of displacive phase transition (PhT) (see Section 2.6). If the A or B atoms are disordered in the PE phase, for example if the B atom is disordered between eight equivalent positions (Figure 2.3a), the relaxation describes the hopping of the B atoms among equivalent potential-energy minima. The middle position of the B-ion is in the center of the cube, i. e., no dipole moment arises and the material is in the PE phase. If the B atoms are ordered in four positions (Figure 2.3b), the middle position shifts along the *c*-direction and tetragonal FE phase with spontaneous polarization $\mathbf{P}_s||[001]$ ($\mathbf{P}_s$ is parallel to [001] plane) is created. Ordering in two positions (see Figure 2.3c), orthorombic FE phase with

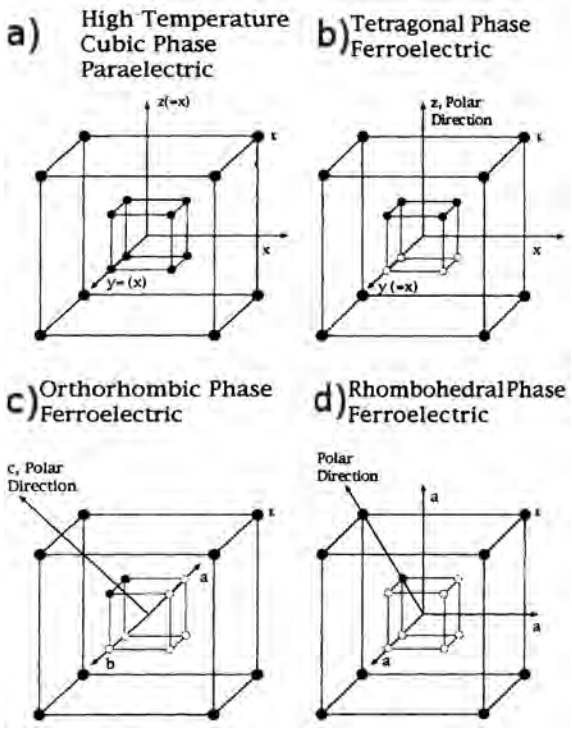

Figure 2.3 Schematic illustration of the B-ion occupation sites within the framework of eight-site model for ABO_3 in each phase (solid circles = lower energy states, open circles = higher energy states) [Dougherty94].

$\mathbf{P}_s$|||[110], and if the B atoms are ordered only in one position (Figure 2.3d) results in rhombohedral FE phase with $\mathbf{P}_s$|||[111] appears. This scheme is frequently used for explanation of phase transition sequence in $BaTiO_3$ or $KNbO_3$. In other perovskites, e. g., in lead perovskites, the Pb atoms in A sites are disordered and B atoms are ordered, but the concept of creation of the FE distortion is qualitatively the same.

2.4 Phonons and Optic Soft Mode

The determination of the complex dielectric function in the IR range has been widely employed in the last 40 years in solid state physics to provide important

information about optical phonons.

The energy of the normal lattice vibrations is quantized, and elementary excitations of energy, $\hbar\omega$, of these vibrations are called phonons, characterized by frequency, ω, and wavevector, $\mathbf{k}$ [Kittel85, Anselm67]. Polar phonons (connected with a change of dipole moment) from the center of Brillouin zone (for wavevector, $\mathbf{k}$, it holds: $\mathbf{k} = \mathbf{0}$) are searched by means of IR spectroscopy. Complementary information of IR spectra is given by Raman spectroscopy, which searches phonons connected with a change of Raman tensor. These two techniques provide usually a complete information about phonon dynamics in the Brillouin zone center. Phonons from the whole Brillouin zone can be investigated only by means of inelastic neutron scattering (INS) and by inelastic X-ray scattering.

The atoms in lattice (particularly in every matter) vibrate accordingly to their temperature. It can be shown [Kittel85] from the analysis of lattice vibrations in the crystal that there are 3 acoustic and $3N - 3$ optical branches, where N is number of atoms in unit cell (the number of sites). These branches are called phonon dispersion curves.

Lyddane, Sachs and Teller derived an equation which connects static, $\varepsilon'(0)$, and high-frequency, ε'_∞ (the dielectric constant in the absence of lattice vibrations, usually at frequencies in near-IR range), permittivity with parameters of polar optic vibrations. In the case of cubic crystals with two atoms per unit cell, the Lyddane-Sachs-Teller (LST) relation has the form

$$\frac{\varepsilon'(0)}{\varepsilon'_\infty} = \left(\frac{\omega_{\mathrm{LO}}}{\omega_{\mathrm{TO}}}\right)^2, \tag{2.7}$$

where ω_{LO} and ω_{LO} are longitudinal and transverse frequency, respectively. Generalized LST relation for crystal has the form [Kittel85, Waser03]

$$\frac{\varepsilon'(0)}{\varepsilon'_\infty} = \prod_{j=1}^{N} \left(\frac{\omega_{\mathrm{LO},j}}{\omega_{\mathrm{TO},j}}\right)^2, \tag{2.8}$$

where N goes over the IR-active modes.

When Curie-Weiss formula (2.6) is put into LST relationship (2.7) and considering ω_{LO} temperature independent, the Cochran law for the soft mode (SM) is

obtained

$$\omega_{\mathrm{TO}} = A\sqrt{T - T_{\mathrm{c}}}, \tag{2.9}$$

where A is a constant. It can be seen that when the temperature goes to T_{c} the frequency of the transverse optical (TO) mode is decreasing—we say the frequency of the mode softens. Therefore, this optic polar mode is called optic soft mode.

Theory of the soft-mode was formulated at the end of the 50's by Cochran [Cochran59], Anderson [Anderson60] and Ginzburg, and represented a major breakthrough in understanding of ferroelectricity. This theory explains the dynamics of the PhTs and shows that they are caused by the lattice instability towards one of the normal lattice vibrations which softens as the temperature goes to the PhT temperature, T_c. The SM concept was very successful and is still valid in elucidating the microscopic mechanism for structural PhTs in general.

Optic SM can be studied by means of FT-IR, Raman spectroscopy and inelastic neutron scattering.

2.5 Low-Frequency Relaxations

Originally the theory of the SM was formulated for displacive PhTs, when the SM is one of the normal lattice vibrations. In a short time similar views on the order-disorder PhTs of anharmonic crystals were confirmed—in this case the SM is not a phonon but a relaxation mode, in microwave (MW) or at lower frequencies, and characterizes anharmonic movement (e. i., cross-jump among potential minima).

Debye derived the formula for the frequency dependence of permittivity of such relaxation [Hench90, Jonscher83],

$$\varepsilon^*(\omega) = \varepsilon'_\infty + \sum_j \frac{\omega_{\mathrm{r},j}\Delta\varepsilon'_j}{\omega_{\mathrm{r},j} + \mathrm{i}\omega}, \tag{2.10}$$

where $\Delta\varepsilon'_j$ is a contribution of the j-th relaxator to static permittivity (in the case of only one relaxator in the spectrum $\Delta\varepsilon' = \varepsilon'_0 - \varepsilon'_\infty$), $\omega_{\mathrm{r},j} = 1/\tau_j$ is the relaxation frequency of the j-th relaxator and τ_j marks its relaxation time.

In some cases the relaxation is broader than predicts Debye formula and the frequency dependence can be rather well fitted with empirical Cole-Cole (1942)

formula [Daniel67, Hench90],

$$\varepsilon^* = \varepsilon'_\infty + \frac{\Delta\varepsilon'}{1 + (\mathrm{i}\omega/\omega_\mathrm{r})^{1-\alpha}}, \tag{2.11}$$

where $\alpha \in (0;1)$ is a parameter characterizing a distribution of relaxation times. In the case of $\alpha = 0$ the relaxation is narrow and Debye formula (2.10) is attained. With α increasing the relaxation is broader, and in the limiting case $\alpha = 1$ the mean relaxation frequency, ω_r, cannot be determined and the relaxation has no peak in the dielectric loss spectrum. In the case of very broad or asymmetric dielectric relaxation, a more general formula is usually used [Fröhlich49, Kamba02],

$$\varepsilon^* = \varepsilon'_\infty + \int \frac{g(\tau)}{1 + \mathrm{i}\omega\tau}\,\mathrm{d}(\ln\tau), \tag{2.12}$$

where $g(\tau)$ is a distribution of Debye relaxation times normalized by the total dielectric strength,

$$\Delta\varepsilon' = \int_0^\infty g(\tau)\,\mathrm{d}(\ln\tau). \tag{2.13}$$

The relaxation lies always below phonon frequencies, and its existence in dielectric spectra gives evidence about some disorder in the dielectric material [Ye98a, Samara01, Samara03]. In most systems the dielectric spectra reveal relaxations slowing down on cooling [Jonscher83], which indicates that the motion of the ions requires a thermally activated hopping over some potential barrier, E_a [Courtens86]. If all charges hop independently of each other and the barrier height is temperature independent, then the relaxation frequency (where a peak in the dielectric loss spectra has its maximum) obeys the Arrhenius law [Jonscher83],

$$\omega_\mathrm{r} = \omega_\infty \exp\left(\frac{-E_\mathrm{a}}{kT}\right), \tag{2.14}$$

where ω_∞ is the relaxation frequency at infinite temperature, T is the temperature, and k marks the Boltzmann constant. In the case of mutually correlated hopping motion, the relaxation frequency obeys the Vogel-Fulcher law [Courtens86, Courtens84],

$$\omega_\mathrm{r} = \omega_\infty \exp\left(\frac{-E_\mathrm{a}}{k(T - T_\mathrm{VF})}\right) \tag{2.15}$$

for $T > T_{VF}$, where the Vogel-Fulcher temperature, T_{VF}, describes the finite freezing temperature of the relaxation, and activation energy, E_a, has the usual meaning (potential barrier) only for $T \gg T_{VF}$.

2.6 Structural Phase Transitions and Their Classification

If a physical system changes its own qualitative property under the changing conditions of external force acting on this system, one can say that this system undergoes PhT. External force can be temperature, pressure, electric and magnetic field, and so on.

PhT can be a change of the state (gas, liquid, solid state), normal-superconductive (normal-superfluid) transition, magnetic PhT, ferroelectric PhT, etc.

Landau had defined a quantity which principally helps to find anomalies of different quantities in the vicinity of PhT—transition parameter η [Landau64, Petzelt76] (also called order parameter). The symmetry of η has a great impact on the PhT order and type.

In historical view there is a classificationf PhTs based on the continuity of thermodynamical potentials into first and second order PhTs.

First order PhT is identified by a jump of the transition parameter, η, from 0 to finite value. It is connected with latent heat, existence of temperature hysteresis and possible phase coexistence in certain temperature range.

Second order PhT is characterized by a continuous change of transition parameter η from 0 (above T_c) to non-zero value below T_c.

If the solid state changes crystal symmetry at some temperature, we call this change the structural PhT. It can be again of first or second order, but another classification is also frequently used.

order-disorder type: Above the PhT temperature, T_c, is some kind of atoms statistically disordered among several equivalent positions, and it orders in some of them below T_c (see Figure 2.3). Final displacement is comparable to atom-atom distances.

displacive type: Some kind of atoms undergoes displacement to another equilibrium position at T_c. The displacement is comparable to amplitudes of the thermal vibrations of atoms; these are essentially smaller than interatomic distances (see Figure 2.2).

2.7 Ferroelectric Phase Transitions and Relaxors

Spontaneous polarization, which can be switched by external electric field (see Figure 2.4a-left), appears below the FE PhT temperature. The FE PhT is always accompanied by dielectric anomaly near T_c and by change of crystal symmetry.

In the case of **proper FE PhT**, the polarization can be taken as transition parameter, η. It shows an abrupt but continuous change at T_c in PhT of second order (see Figure 2.4b-left). In the case of the first order PhT a finite jump of $\mathbf{P}_s$ creates at T_c. The permittivity, $\varepsilon'(T)$, obeys the Curie-Weiss law (2.6) above the PhT temperature (Figure 2.4c-left). Curie-Weiss temperature corresponds to PhT temperature at second order PhT, in the case of first order PhT the Curie-Weiss temperature is slightly shifted below the PhT temperature.

The optical SM is IR active both above and below T_c and Raman active always at least below T_c. There are also **improper FE PhT**, where the polarization has different symmetry than the transition parameter, which is usually a SM from Brillouin zone boundary. Doubling or even higher multiplication of unit cells occurs below T_c. Permittivity does not follow the Curie-Weiss law, only a jump in $\varepsilon'(T)$ occurs at T_c. Because the soft mode is from Brillouin zone boundary, it is not IR active above T_c, but it is activated in the IR spectra below T_c. The SM can be studied above T_c only by means of INS.

Special case is **pseudoproper PhT**, where the transition parameter is not polarization, but polarization is of the same symmetry. In this case only weak Curie-Weiss dielectric anomaly near T_c occurs.

If the material is macroscopically heterogeneous with some distribution of T_c, the maximum in $\varepsilon'(T)$ is rounded and polarization persists for a short range of temperatures above the temperature of permittivity maximum, T_m. This kind of PhT is called **diffuse PhT**.

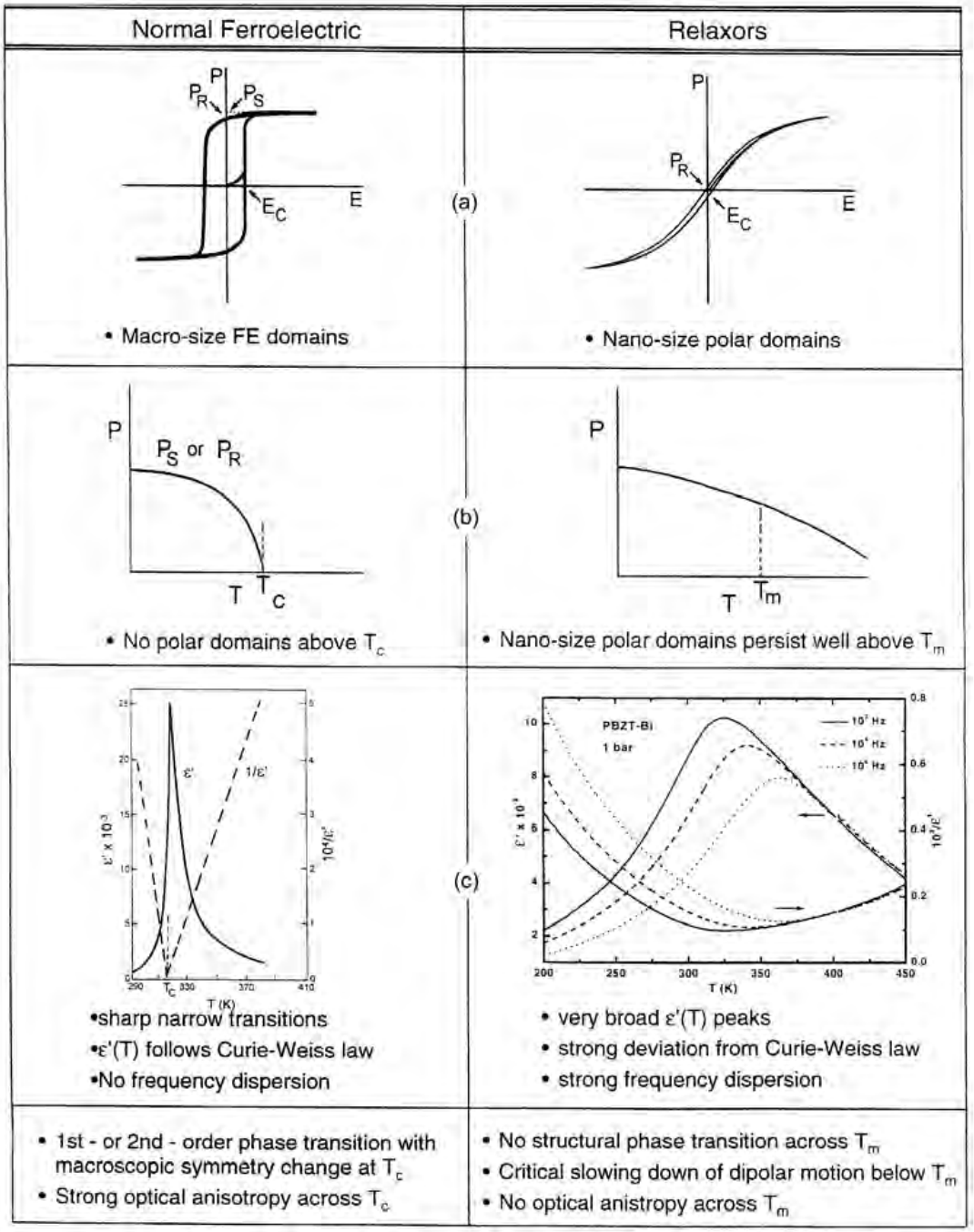

Figure 2.4 Contrast between the properties of normal FEs and relaxors, [Samara03].

There is a special kind of diffuse FEs—relaxor ferroelectrics, or relaxors. There are some special properties of FE relaxors and **relaxor FE PhTs** [Ye98a, Cross94]:

- Relaxors are characteristic by high and broad maxima of real and imaginary parts of the complex permittivity, which shift with increasing measuring frequency to higher temperatures (Figure 2.4c-right).
- The transition is clearly diffuse, 'rounded' and T_m is a function of frequency. Dielectric response is markedly dispersive below T_m.
- Curie-Weiss dependence (2.6) of the permittivity is seen only far above T_m and strong deviations from this law appears for $T \leq T_d$ ($T_d \gg T_m$) (Figure 2.4c-right).
- The relaxors do not possess necessarily a macroscopic polarization (Figure 2.4a-right), but local non-zero polarizations associated with the polar nanoregions (nanoclusters). The temperature at which nanoclusters start to exist is called Burns temperature, T_d (Figure 2.4b-right).
- Below the freezing temperature, T_{VF}, flowing from Vogel-Fulcher law (2.15), the polar clusters (nanoclusters) are frozen, i. e., the polarization in clusters does not flip unlike above T_{VF}. Only cluster-wall motion can contribute to permittivity below T_{VF}.
- There is a non-Debye dielectric dispersion for $T \lesssim T_m$ and in many cases a frequency-independent dielectric loss for $T \ll T_m$ was observed.
- Diffuse and frequency dependent ε' near T_m can be explained by non-Debye (broad) dielectric relaxation (2.11) which slows down and broadens on cooling.

There is a large number of compounds that show relaxor ferroelectric behavior [Ye98a] and most of them have perovskite structure.

Chapter 3

Experimental Techniques

Methods that were used in experiments of this work to collect the MIR, FIR, THz, MW and HF spectra of the investigated material were as follows:

- high-frequency (HF) dielectric spectroscopy,
- time-domain terahertz spectroscopy (TDTS), and
- Fourier transform infrared spectroscopy (FT-IR).

3.1 High-Frequency Dielectric Spectroscopy

The basic principles of this technique were developed quite a long time ago, in spite of it the technique is still not so widely used as the conventional radio-frequency devices, whose upper frequencies are limited by $\sim 1\,\mathrm{MHz}$, because the dielectric parameters has to be calculated taking into account the electromagnetic (EM) field distribution in the sample [Grigas96]. The second problem is that the high permittivity samples must have a special geometry, usually long sticks ($> 5 - 8\,\mathrm{mm}$) of cylindrical shape with a small diameter ($< 1\,\mathrm{mm}$).

Dielectric measurements in the HF range of $1\,\mathrm{MHz} - 1.8\,\mathrm{GHz}$ were performed using a computer controlled dielectric spectrometer equipped with an Agilent

4291B Impedance-Material Analyzer, a NOVOCONTROL BDS 2100 coaxial sample cell and a SIGMA SYSTEM M18 temperature chamber (operating temperature range $100 - 570\,\mathrm{K}$)—our experiment was performed in the temperature region $100 - 500\,\mathrm{K}$. The temperature variation rate for all data sets that will be discussed, was kept at $1\,^{\circ}\mathrm{C/min}$. Since the frequency sweep time is 5 s, the data collected during one sweep were considered as measured at the same temperature (see also [Porokhonskyy04]).

The conventional relation between the sample capacity and complex dielectric constant, ε^*, was obtained as a limit of a more general solution, where spatial variation of EM field was taken into account [Porokhonskyy04]. But it can be shortly said that firstly the frequency and temperature dependencies of the impedances of the samples have been measured first and then the complex permittivities have been evaluated.

3.1.1 Characterization of Samples Used for High-Frequency Dielectric Spectroscopy

The diameters of the 8 mm long sticks of cylindrical shape were (in order of $PbTiO_3$ (PT) concentration: $x = 0, 0.25, 0.37$) 510 µm, 550 µm and 500 µm, respectively.

3.2 Time-Domain Terahertz Spectroscopy

TDTS is a recently introduced (20 years ago) and now well-established method of material science. It covers a broad frequency range extending from tens of GHz up to few THz (up to FIR range), thus bridging a large gap between MW and conventional IR spectroscopies, depending on the techniques [Pashkin04, Kužel04]. Moreover, as a phase-sensitive method, TDTS provides a direct access to both real and imaginary part of the dielectric function of the studied material with no need to perform the Kramers-Kronig analysis and with no *a priori* fitting model.

The technique (Figure 3.1) requires to measure the temporal profile of the electric field of a THz pulse transmitted through the investigated sample [Kužel00]. The Ti:sapphire femtosecond laser ("Mira Seed" by COHERENT), in modified

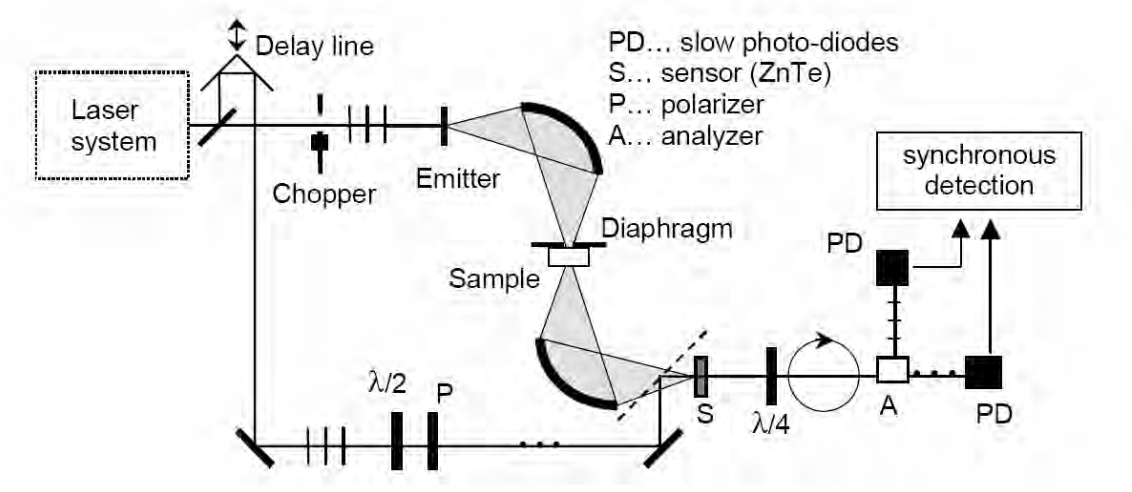

Figure 3.1 TDTTS experimental scheme

passive mode-locking regime, so called "self-locking", generates a femtosecond pulse (the characteristics of the generated ultrashort light pulses: pulse length: $50-80$ fs, spectral bandwidth: $15-40$ nm, repetition rate: 76 MHz, energy per pulse: 8 nJ, average power 650 mW, pulse peak power: 140 kW). Quantronix "Odin" multipass femtosecond amplifier allows to amplify the generated pulses (pulse length: 50 fs, spectral bandwidth: 30 nm, repetition rate: 1 kHz, energy per pulse: 1 mJ, average power: 1 W, pulse peak power: 25 GW). The optic pulses come to emitter and there a ZnTe crystal produces THz radiation through optical rectification under phase-matching conditions in the frequency range from 100 GHz up to 3 THz. In contrast to common methods of optical spectroscopy, which determine the time average of the radiation intensity, TDTS measures a time profile of THz pulse EM field. The phase shift establishment is done by scanning the position of the delay line, which corresponds to the time delay between the THz pulse and the sampling beam. The signal is detected by a sensor from ZnTe crystal, using electro-optic detection.

Terahertz data give complementary information in very difficult spectral range and in combination with other two methods of dielectric spectroscopy (HF and FT-IR) they allow us to improve the quantitative picture of dielectric response in

a broad frequency range.

In our setup the lowest frequency which could be detected and/or generated was about 0.1 THz ($\lambda = 3$ mm), but the lowest frequency we could trust with our samples was about 0.3 THz ($\lambda = 1$ mm). The reason was the relatively low transmissivity in the material at low frequencies due to high absorption and the consequent inaccuracy. On the ground of the largest used wavelength 1 mm, the beam and the EM field of the beam was not disturbed with an aperture with diameter 4 mm, which was the smallest one we used. The highest frequency, which can be reached in our TDTS setup, is about 2.5 THz ($\nu = 80\,\mathrm{cm}^{-1}$), but in real case it is determined by a value of transmissivity of the sample in this frequency range (FR).

3.2.1 Samples Characterization for TDTS

Thickness of the samples and the aperture diameter used were in range $24 - 27\mu$m and $4 - 8$mm, respectively. Plane parallelity of $\sim 1\,\mu$m was acquired. The samples were prepared so thin, because of high absorption coefficient in our studied ceramics.

3.3 Fourier Transform Infrared Spectroscopy

FT-IR spectroscopy is a method which in principle covers a broad spectral range from FIR to visible range. Unlike a dispersive instrument, i. e., an instrument with grating monochromator, FT-IR spectrometer collects all wavelengths simultaneously. This feature is called the multiplex or Felgett advantage. The FT-IR is a method of obtaining IR spectra by first collecting an interferogram of a sample signal using an interferometer, and then performing a Fourier Transform on the interferogram to obtain the spectrum. The FT-IR is typically based on a Michelson interferometer (Figure 3.2). The interferometer consists of a beam splitter, a fixed mirror, and a mirror that translates back and forth, very precisely.

The interferogram acquired by an FT-IR spectrometer has a center burst (Figure 3.3). Its origin lies in the fact that all wavelengths are in-phase at the zero path difference in interferometer. As the optical path difference grows, different

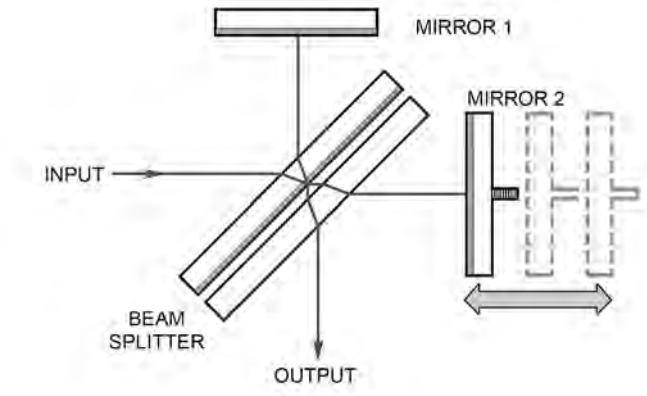

Figure 3.2 Michelson interferometer. The mirror 2 translates back and forth, thereby causing phase shifts among frequencies.

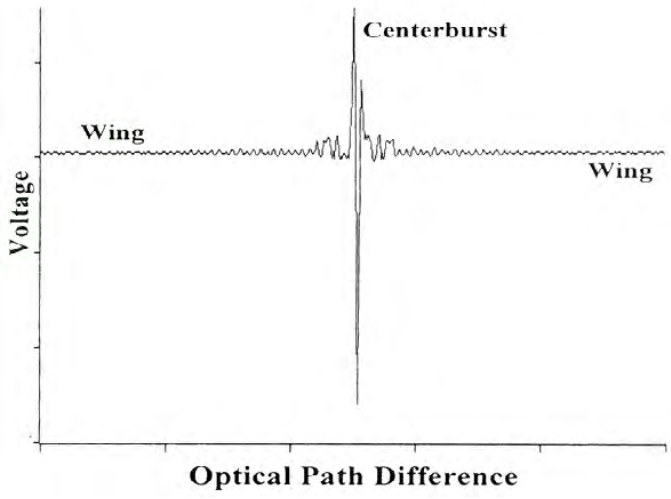

Figure 3.3 Common interferogram

wavelengths produce peak readings at different positions and, for a broadband signal, they never again reach their peaks at the same time, as happened in center burst. The x-axis of the interferogram represents the optical path difference.

Once an interferogram is collected, the translation into a spectrum (emission, absorption, transmission, etc.) is done through the Fast Fourier Transform al-

gorithm (method by J. W. Cooley and J. W. Tukey, 1965). The mathematics and principles of the FT-IR spectroscopy is deeply discussed in [Bell72].

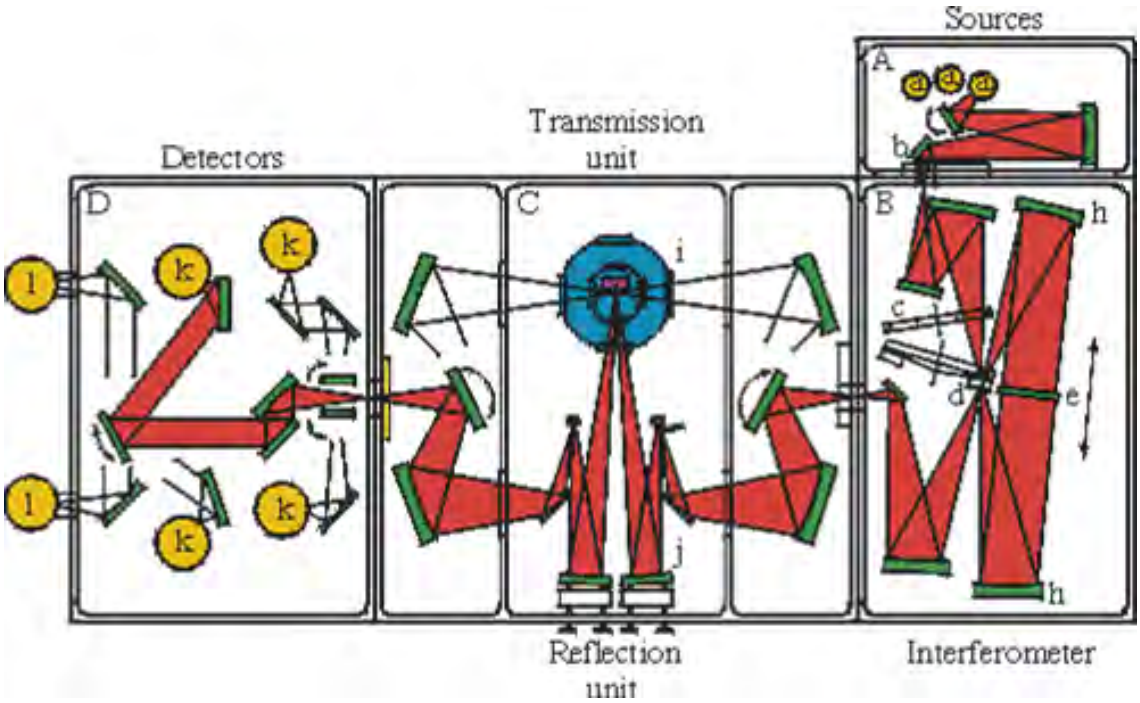

Figure 3.4 Scheme of Spectrometer Bruker IFS-113v: (A) source chamber, (a) sources, (B) chamber of interferometer, (c) filters, (d) beamsplitters, (e) movable mirror, (h) mirrors, (C) sample chamber, (i) sample, (j) mirrors, (D) detector chamber, (k) detectors and (l) outside detectors.

For measurements in the IR FR the spectrometer Bruker IFS-113v was used. Mercury lamp emission was used as the source of FIR radiation (see scheme in Figure 3.4), black polyethylene filter below $700\,\mathrm{cm}^{-1}$, KBr beamsplitter covered with Ge thin film (in $400 - 4000\,\mathrm{cm}^{-1}$) and T222, 6 µm thick Mylar covered with antireflex film ($30 - 650\,\mathrm{cm}^{-1}$) was used.

A helium-cooled Si bolometer operating at 1.5 K was used as a detector during measurement with cryostat and deuterated triglycine sulfate detector at $T >$ 300 K. Helium-cooled Optistat CF cryostat with polyethylene windows was used

for cooling down to 20 K and home-made furnace for heating, from room-temperature (300 K) to 20 K and 550 K, respectively. (For further particulars see also [Ostapchuk04, Buixaderas01].)

3.3.1 Unit Conversion in IR and THz Spectroscopy

The relation between IR wavelength, λ, and frequency, f, is given by the following relationship:

$$\lambda = c_0/f, \tag{3.1}$$

where c_0 is a speed of light in vacuum. Another unit which is frequently used in IR spectroscopy is wavenumber, $\nu[\mathrm{cm}^{-1}]$. Its relation to wavelength and frequency is as follows:

$$\nu = \frac{1}{\lambda} = f/c_0 \tag{3.2}$$

The conversion between wavenumber and frequency is as follows:

$$3 \times 10^{10}\nu[\mathrm{cm}^{-1}] = f[\mathrm{Hz}] \tag{3.3}$$

3.3.2 Fitting Models

Permittivity in IR region cannot be measured directly, it is customarily obtained from the measured reflectance, R, or transmittance spectrum of the material. In the case of opaque sample only reflectivity can be measured and permittivity is obtained from the fit of reflectivity by means of formula (valid in the case of near normal reflectivity)

$$R(\omega) = \left| \frac{\sqrt{\varepsilon^*(\omega)} - 1}{\sqrt{\varepsilon^*(\omega)} + 1} \right|^2, \tag{3.4}$$

which can be rewritten (using (2.3), the frequency dependencies are omitted)

$$R = \frac{1 + \sqrt{\varepsilon'^2 + \varepsilon''^2} - \sqrt{2\left(\varepsilon' + \sqrt{\varepsilon'^2 + \varepsilon''^2}\right)}}{1 + \sqrt{\varepsilon'^2 + \varepsilon''^2} + \sqrt{2\left(\varepsilon' + \sqrt{\varepsilon'^2 + \varepsilon''^2}\right)}}. \tag{3.5}$$

When the splitting between TO and longitudinal optical (LO) modes of the phonon is weak (the IR reflection bands are narrow), the dielectric function is assumed to be a sum of N damped harmonic oscillators,

$$\varepsilon^*(\omega) = \varepsilon'(\omega) - \mathrm{i}\varepsilon''(\omega) = \varepsilon'_\infty + \sum_{j=1}^{N} \frac{\Delta\varepsilon'_j \omega^2_{\mathrm{TO},j}}{\omega^2_{\mathrm{TO},j} - \omega^2 + \mathrm{i}\omega\gamma_{\mathrm{TO},j}}, \tag{3.6}$$

where $\omega_{\mathrm{TO},j}$, $\gamma_{\mathrm{TO},j}$ and $\Delta\varepsilon'_j$ are eigenfrequencies, dampings and dielectric strengths of the oscillators, respectively. Otherwise, four-parameter generalized oscillator model is essential [Berreman68]:

$$\varepsilon^*(\omega) = \varepsilon'_\infty \prod_{j=1}^{n} \frac{\omega^2_{\mathrm{LO},j} - \omega^2 + \mathrm{i}\omega\gamma_{\mathrm{LO},j}}{\omega^2_{\mathrm{TO},j} - \omega^2 + \mathrm{i}\omega\gamma_{\mathrm{TO},j}}, \quad \left(\Delta\varepsilon'_j = \frac{\varepsilon'_\infty}{\omega^2_{\mathrm{TO},j}} \frac{\prod_k \left(\omega^2_{\mathrm{LO}k} - \omega^2_{\mathrm{TO},j} \right)}{\prod_{k\neq j} \left(\omega^2_{\mathrm{TO}k} - \omega^2_{\mathrm{TO},j} \right)} \right), \tag{3.7}$$

where transverse, $\omega_{\mathrm{TO},j}$, and longitudinal, $\omega_{\mathrm{LO},j}$, optic phonon frequencies are > 0. $\omega_{\mathrm{TO},j}$ is shown by maxima of the peaks in $\varepsilon''(\omega)$, $\omega_{\mathrm{LO},j}$ is defined from $\varepsilon^* = 0$, $\gamma_{\mathrm{LO},j}$ and $\gamma_{\mathrm{TO},j}$ are dampings of the oscillators (see Figure 3.5).

Figure 3.5 shows the shape of various kind of spectra (R, T, ε', ε'', n and κ) of one optic phonon mode, which is fitted by means of one four-parameters generalized oscillator. The big ratio of TO and LO damping affects the symmetry of dielectric loss spectra, ε'', and transmissivity spectra, as can be seen.

3.3.3 Samples Characterization for IR Measurements

The raw samples were cut and polished on one side (roughness $\sim 0.1\,\mu\mathrm{m}$) for reflectivity measurements. The thickness and the diameter of the pellets were about 2 mm and 8 mm, respectively. Because of the large thickness and the rough opposite side interference was not present in the spectra.

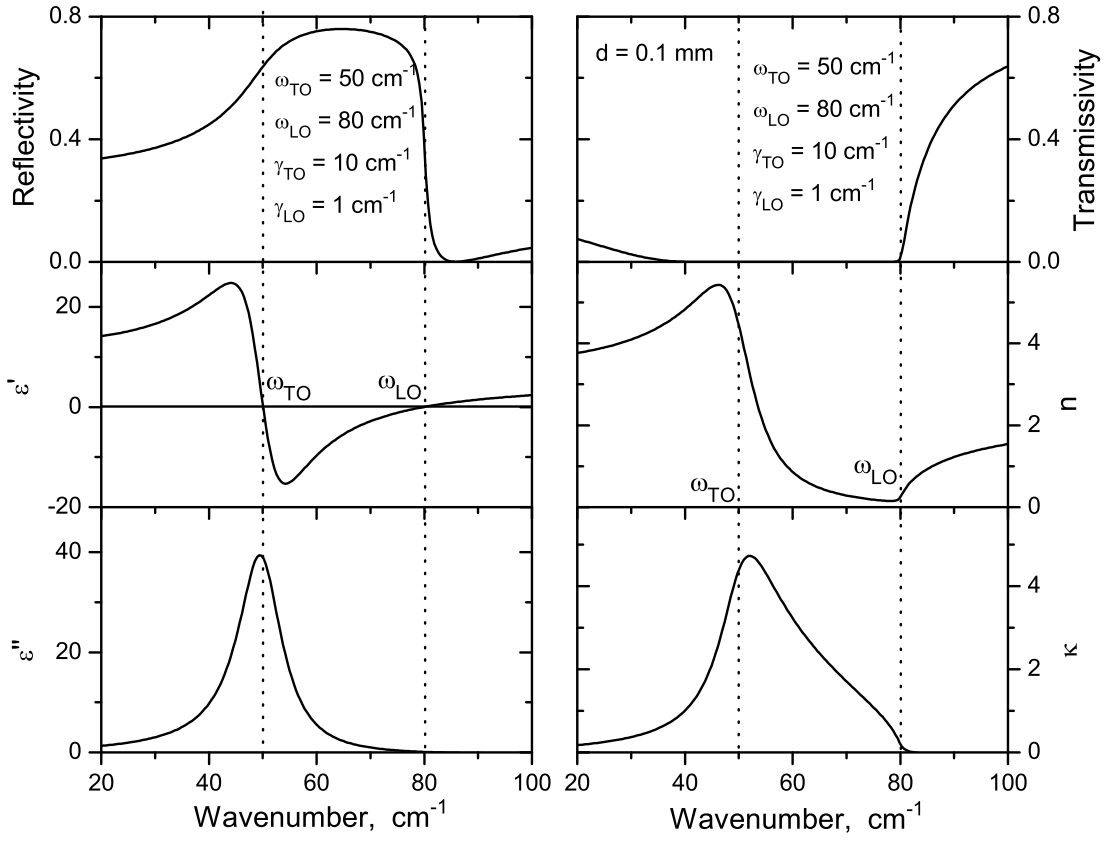

Figure 3.5 Calculated reflectivity, permittivity (ε'), diel. loss (ε''), trasmissivity (for a thickness 0.1 mm), real (n) and imaginary (κ) parts of the refractive index for one oscillator with parameters $\omega_{\mathrm{TO}} = 50\,\mathrm{cm}^{-1}$, $\omega_{\mathrm{LO}} = 80\,\mathrm{cm}^{-1}$, $\gamma_{\mathrm{TO}} = 10\,\mathrm{cm}^{-1}$, $\gamma_{\mathrm{LO}} = 1\,\mathrm{cm}^{-1}$ and $\varepsilon'_\infty = 5$.

Chapter 4

Material Characterization and Experimental Results

4.1 $Pb(Fe_{2/3}W_{1/3})O_3$-$PbTiO_3$ Characterization

In the last years there has been an increasing interest in perovskite solid solutions formed by relaxor $Pb(B'_{1-x}B''_x)O_3$, where B′ is a low valence cation (Mg^{2+}, Zn^{2+}, and Fe^{3+}), B″ a high valence cation (Ti^{4+}, Nb^{5+}, and W^{6+}) and the FE $PbTiO_3$ (PT), because their single crystals exhibit giant piezoelectricity response [Park97]. Relaxor ferroelectrics $Pb(Mg_{1/3}Nb_{2/3})O_3$ (PMN), $Pb(Zn_{1/3}Nb_{2/3})O_3$ (PZN) and $Pb(Sc_{1/2}Ta_{1/2})O_3$ and their solid solutions with PT are the most investigated systems. They were studied in single crystal, thin film, or ceramic forms.

The phase diagrams of these solid solutions are rather complicated, but have some common features. At high temperatures they crystallize in cubic phase, at lower temperatures a PhTs to the FE rhombohedral (because of low PT concentration) or to the tetragonal (because of large PT concentration) phase occurs. The phase boundary between the rhombohedral and tetragonal phase is almost temperature independent. This boundary is called morphotropic phase boundary (MPB) and optimum dielectric and piezoelectric properties have been found here, justifying the present interest to study the MPB phenomena in other systems, like our $Pb(Fe_{2/3}W_{1/3})O_3$-$PbTiO_3$.

A solid solution between relaxor ferroelectric $Pb(Fe_{2/3}W_{1/3})O_3$ (PFW) and

FE PT, $(1-x)$PFW-(x)PT, has been synthesized and characterized in detail by means of X-ray diffraction in the whole concentration range, $x \in (0;1)$, [Feng02, Mitoseriu02c]. A phase diagram was established (Figure 4.1) and MPB between rhombohedral and tetragonal phase investigated [Mitoseriu02a, Mitoseriu02b].

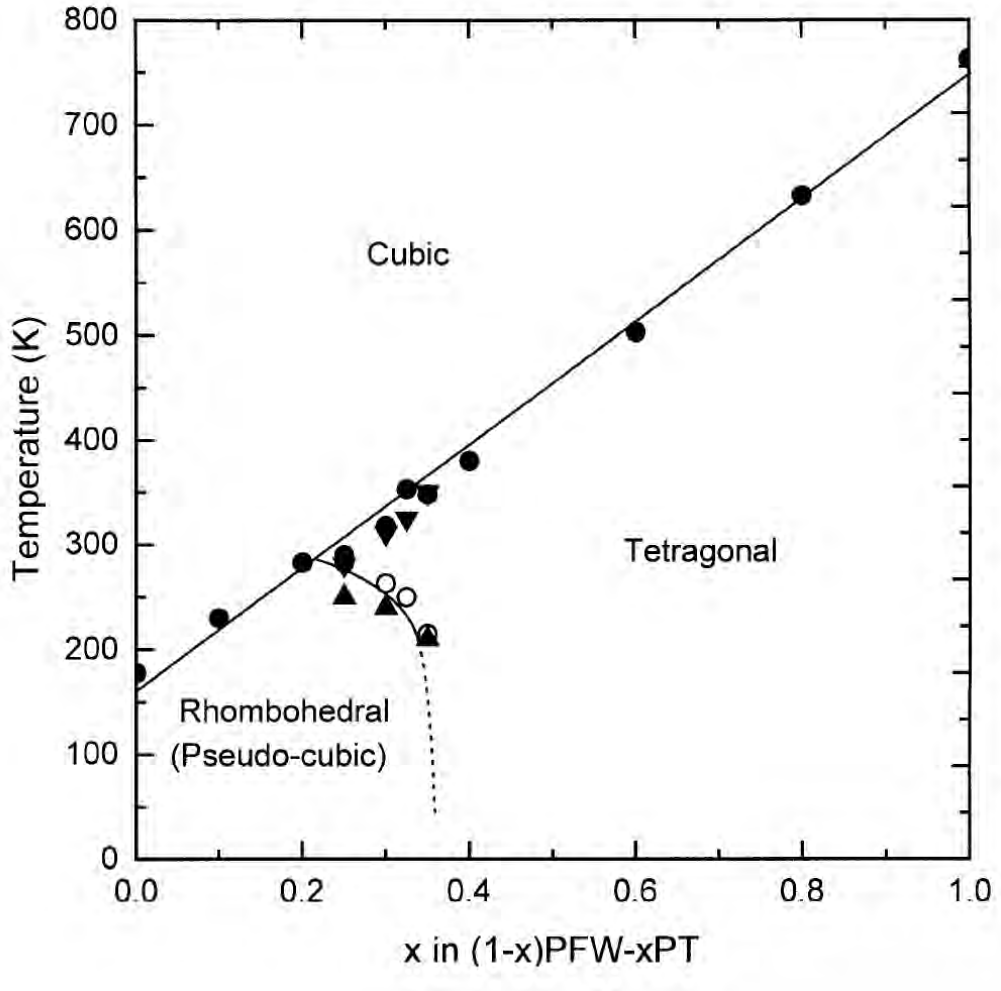

Figure 4.1 Phase diagram of the $(1-x)$PFW-(x)PT system delimiting the high-temperature cubic phase and the low-temperature rhombohedral (pseudocubic) and tetragonal phase [Feng02].

Previous dielectric studies [Mitoseriu02a, Vilarinho02, Feng02, Mitoseriu03c] on the $Pb(Fe_{2/3}W_{1/3})O_3$-$PbTiO_3$ (PFW-PT) have shown that as the PT concentration increases the temperature of the dielectric permittivity maximum increases

and the system gradually loses the relaxor behavior and becomes a normal FE for $x > 0.25$. These measurements were mostly done in the low- (audio- and radio-) [Vilarinho00, Schevchuk97] and briefly in the high-frequency [Schevchuk99, Schevchuk97] range by means of dielectric spectroscopy at low (cooling down to 100 K), room- and high temperatures (heating up to 600 K). Lattice dynamics and phonon anomalies near T_c were studied by means of Raman scattering [Mitoseriu04]. Structure changes and the coexistence of phases near MPB were performed by means of X-ray diffraction [Mitoseriu02c] and differential scanning calorimetry [Feng02]. Modified Landau theory was applied for explanation of relaxor behavior in pure PFW [Mitoseriu03c, Mitoseriu03b].

Pure PFW exhibits also two magnetic PhTs near 20 K and 350 K, the magnetic properties of PFW and PFW-PT were published in [Ye98b] and [Mitoseriu03a], respectively.

4.1.1 Phase Diagram

Pure PFW is a ferroelectric relaxor with disordered ABO_3 perovskite structure, in which Fe^{3+} and W^{6+} ions are randomly distributed in B-sites of the BO_6 octahedral positions (see Section 2.3.1) and Pb atoms are disordered in A-sites [Ye98a].

PFW exhibits a diffuse and frequency dependent dielectric permittivity maximum at low temperatures ($\sim$ 185 K), i. e., much lower (by about 100 K) than in other relaxors like PMN, PZN, etc. The temperature dependencies of the permittivity at various frequencies have revealed that the FE PhT temperature T_c increases with the increasing Ti^{4+} content on the B-site, and the relaxor FE behavior of PFW is gradually transformed into normal (long-range) FE state in PFW-PT, as evidenced by the sharp and non-dispersive dielectric peaks around T_c for $x \geq 0.25$ [Feng02].

A MPB is located within the composition interval $0.25 \leq x \leq 0.35$, which separates the pseudocubic (rhombohedral) phase from the tetragonal phase. This MPB is not so sharp like in PMN-PT or PZN-PT solid solution and in contrast to them no additional intermediate monoclinic or orthorombic phase has been observed in it [Mitoseriu02a].

Unfortunately, this system shows rather high conductivity in low-frequency (LF) range even at temperatures below room temperature, which disturbs the LF dielectric data near T_m. An advantage of HF measurements, which were not yet performed, is the absence of conductivity in broad temperature region (up to 500 K). Dielectric response is not disturbed near T_c with high conductivity and more accurate data can be obtained. This was a motivation for our HF dielectric study.

4.2 System and Samples Preparation

$(1-x)$PFW-(x)PT ceramics with various PT contents ($x = 0.0, 0.25, 0.37$) were prepared using a conventional mixed oxide method at the University Aveiro, Portugal, [Mitoseriu02b, Vilarinho00]. Stoichiometric proportions of the starting oxides PbO, Fe_2O_3, WO_6 and TiO_2 (Merck, min. purity of 99%) were mixed, milled (in ethanol for 6 h), dried and calcinated (for 3 h at 850 °C). The calcinated powders were milled again (for $8-10$ h) to obtain powders of < 5 µm particle size. Pellets (10 mm in diameter, $2-3$ mm in thickness) were pressed isostatically at 250 MPa and the sintering was conducted at about 1200 K for 3 h. The ceramics used by us have porosity less than 4 %.

4.3 Experimental Data of Pure PFW

Figure 4.2 shows the temperature dependencies of permittivity, ε', and dielectric loss, ε'', of pure PFW at various frequencies. There is a remarkable frequency dependence (dispersion) in the temperature range from 100 K to 230 K and above 300 K in the whole measured FR. The peaks of the permittivity are broad and almost symmetrical below 300 K, and the temperature of the permittivity maximum, T_m, grows with increasing frequency and varies from 180 K at 1 MHz to 220 K at 1 GHz. At the same time the position and the intensity of the dielectric loss peak increases with frequency. The dielectric dispersion near T_m reflects a typical relaxor FE behavior (see Section 2.7) arising from the responses of polar nanoclusters [Ye98a].

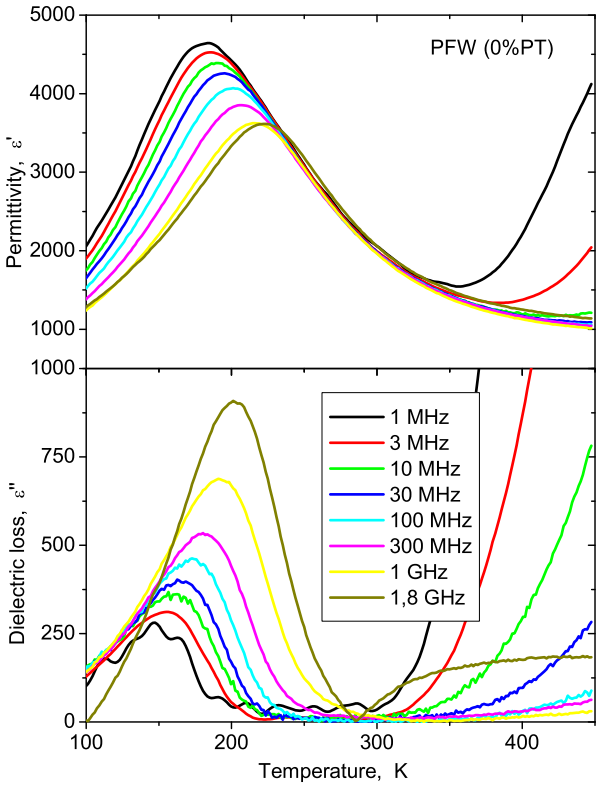

Figure 4.2 Temperature dependencies of permittivity and dielectric loss of pure PFW at various frequencies.

Vogel-Fulcher fit (2.15) was applied to the temperature dependence of frequencies, ω_m, where permittivity exhibits maxima. The accurate fit was obtained (see Figure 4.3), and we got the freezing temperature at $T_{VF} = 170 \pm 5\,K$, $\omega_\infty = 100 \pm 50\,GHz$ and $E_a/k = 220 \pm 50\,K$. The dielectric strength of this relaxation, $\Delta\varepsilon'$, shows that the relaxation is responsible for the huge dielectric anomaly at T_m.

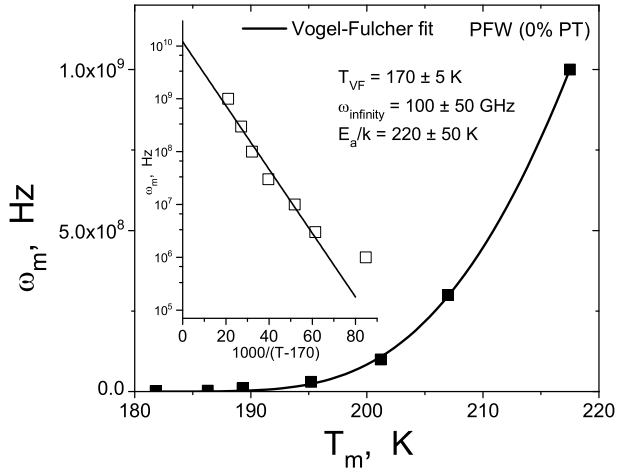

Figure 4.3 Temperature dependence of frequencies at which permittivity maxima in pure PFW occur fitted by means of Vogel-Fulcher formula. Inset is the Vogel-Fulcher plot, $\omega_m \left(\frac{1000}{T-T_{VF}}\right)$.

In the high-temperature paraelectric phase ($T > T_c$), another frequency dispersion appears, which is particularly significant at low frequencies. Such low-frequency dispersion can be attributed to the conductivity effects due to slowly mobile electronic charges [Bovtun05, Feng02]. It is so significant that the "real" permittivity determination (without the contribution of the conductivity) were impossible, but we were not interested in studying it, because of no dramatic changes of complex permittivity in the frequency range below 10 MHz.

In Figure 4.4 we present the frequency dependencies of the permittivity and the dielectric loss obtained from the HF experiment at selected temperatures. Some dispersion at lower frequencies (below 10 MHz) and higher temperatures (above 350 K) is assigned to conductivity, as discussed above.

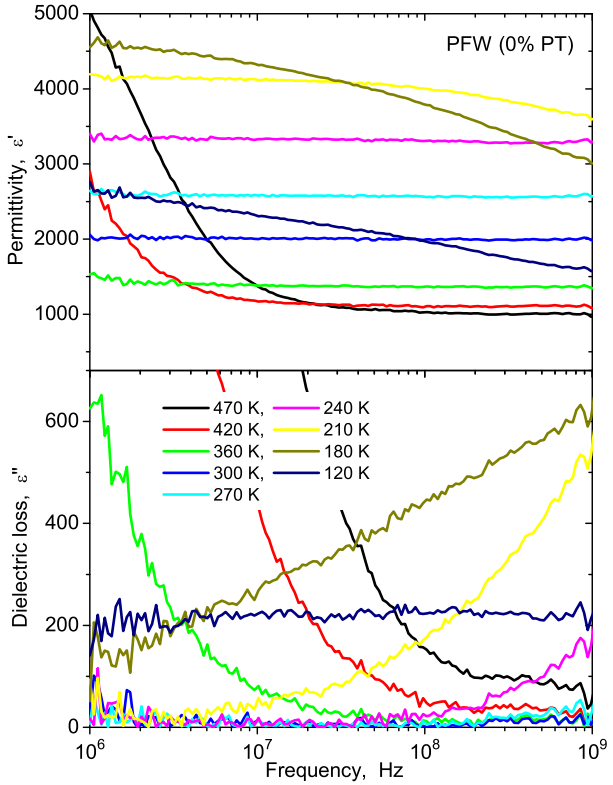

Figure 4.4 Frequency dependence of high-frequency data of PFW, on the right the relaxation, on the left conductivity appears.

It can be seen that some dispersion above 100 MHz begins at temperatures below 270 K (look the increase of $\varepsilon''(\omega)$) near 1 GHz. It is the low-frequency wing of relaxation with relaxation frequency above 1 GHz. The relaxation frequency decreases, i. e., slows down, on cooling. Finally high dielectric loss with no significant maximum is seen at 120 K, which manifests itself as a broad distribution of relaxation times, typical feature of relaxator FEs.

In spite of no visible relaxation peak in the HF range, THz data, measured in the temperature range $20 - 300$ K and in the FR $0.3 - 1.3$ THz, helped us to make the Cole-Cole fits (2.11) in the temperature range $190 - 260$ K. Parameters of the relaxator at various temperatures are shown in Figure 4.5 and 4.6, together with the Arrhenius fit of the main relaxation frequency. The parameters of Arrhenius fit were evaluated, $\omega_\infty = 88 \pm 47$ THz and $E_a/k = 1890 \pm 130$ K. The strength

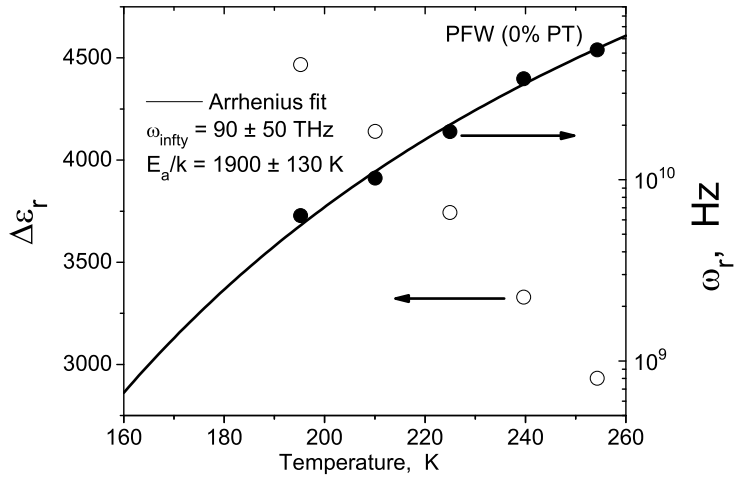

Figure 4.5 Arrhenius fit (2.14) applied on relaxation frequencies of relaxator we have got from Cole-Cole fits with united HF and THz data.

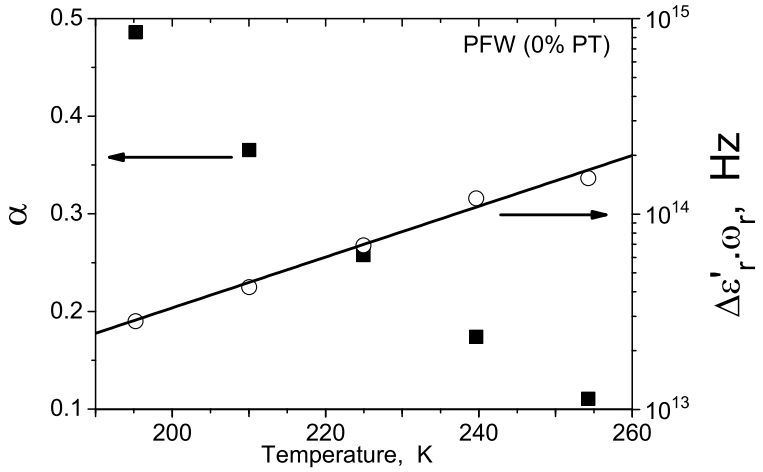

Figure 4.6 Dependence of relaxator parameters α and $\Delta\varepsilon'_r \cdot \omega_r$ (strength), incident in MW range, from fitting with Cole-Cole formula. Note the logarithmic scale for strength.

of the relaxator, $\Delta\varepsilon'_r \cdot \omega_r$, is temperature dependent, which gives evidence about the coupling of this relaxation with another relaxation or phonon. The increas of α on cooling manifests itself by a broadening of the distribution of relaxation frequencies.

It is interesting to note that we did not observe the Vogel-Fulcher behavior of the relaxation frequency in contrast to other relaxators like PMN [Bovtun04]. Nevertheless, our Arrhenius behavior can be obtained as a direct consequence of gradual (Arrhenius) broadening of the distribution of relaxation frequencies with decreasing temperature [Tagantsev94].

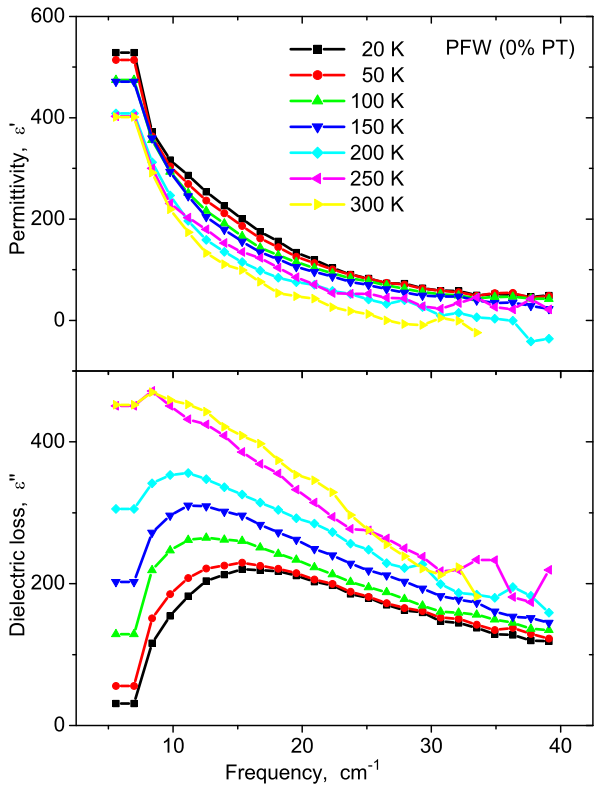

Figure 4.7 Measured THz data of PFW in frequency range $0.3 - 1.3$ THz.

A rapid growth of permittivity in THz data below $10\,\mathrm{cm}^{-1}$ (see Figure 4.7) can be caused by a second relaxator in MW range. Due to very low transparency of the sample at the low frequencies and the high inaccuracy of $\varepsilon^*(\omega)$, we decided to omit data below $15\,\mathrm{cm}^{-1}$ and considered only one relaxation with relaxation frequency within the FR $1 - 100$ GHz at temperatures between 100 K and 300 K.

The IR data were collected in the IR region, $20 - 700\mathrm{cm}^{-1}$, with a resolution $2\,\mathrm{cm}^{-1}$, at temperatures between 20 K and 550 K (see Figure 4.8). The room-

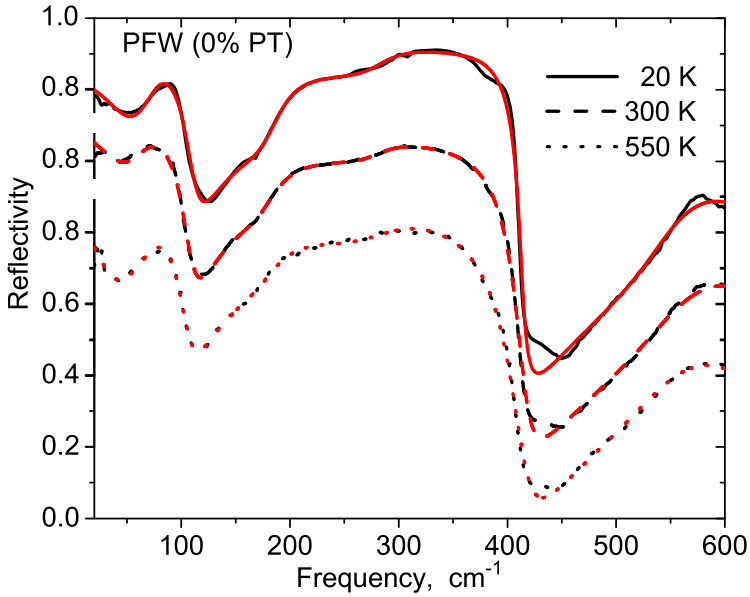

Figure 4.8 Measured (black line) and calculated (red line) reflectivity of PFW for selected temperatures 20 K, 300 K and 550 K.

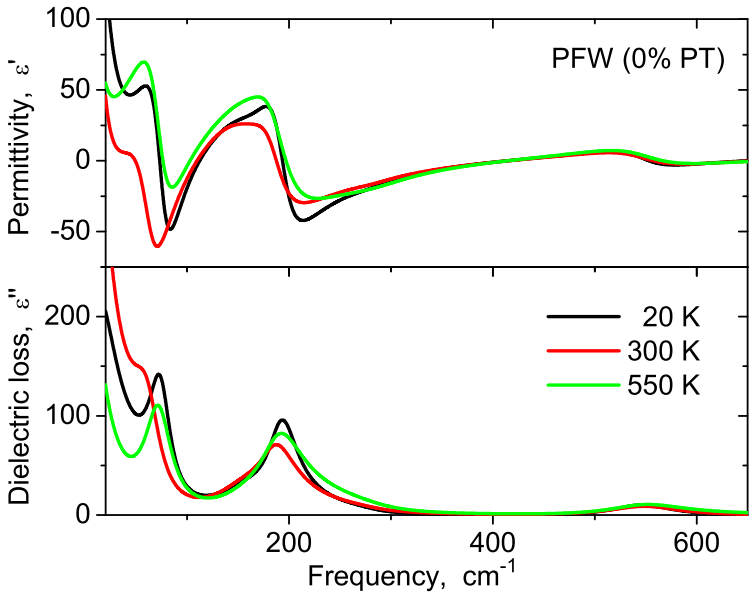

Figure 4.9 Calculated permittivity and dielectric loss of PFW.

temperature spectra were measured up to 3000 cm^{-1}, but all the important spectral features due to the phonon absorption are seen below 700 cm^{-1}.

The IR reflectivity spectra were fitted with the four-parameter generalized oscillator model (3.7), the MW relaxation was fitted in the first approximation by three-parameter overdamped ($\gamma_{TO} > \omega_{TO}$) oscillator (3.6), expressing the increase of reflectivity below 50 cm^{-1}. The experimental data and fitted curves of reflectivities and the components of complex permittivity are depicted for temperatures 20 K, 300 K and 550 K in Figure 4.8 and 4.9, respectively.

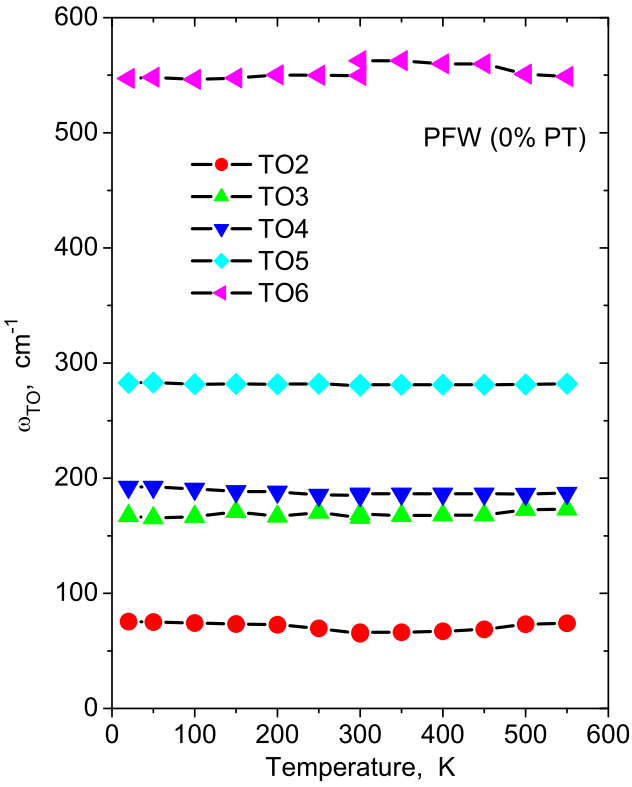

Figure 4.10 Transverse optic phonon frequencies in IR range of PFW were obtained by means of four-parameter generalized oscillator model (3.7). TO1 frequency is omitted in the plot, because it represents the frequency of overdamped oscillator (not phonon) roughly describing the increase of reflectivity below 50 cm^{-1}.

In Figure 4.10 we present the temperature dependencies of the TO frequencies of the fitted phonons. No remarkable anomalies with temperature are seen. The

discontinuity of the 6th phonon at room-temperature is caused by non-continuous fitting. The data from 20 K to 300 K and from 300 K to 550 K were collected with different techniques and fitted separately from each other. No optic SM was observed, which gives evidence that only slowing down of MW relaxation is responsible for the relaxor behavior of PFW.

The extension of the fits into the MW FR can be seen in Figure 4.11 where the complete dielectric spectra obtained from the HF, THz and IR spectra are shown. In spite of using classical damped oscillator in the MW range, pretty good correlation between the HF, THz and IR spectra were achieved by means of classical damped (overdamped) oscillator model as relaxator.

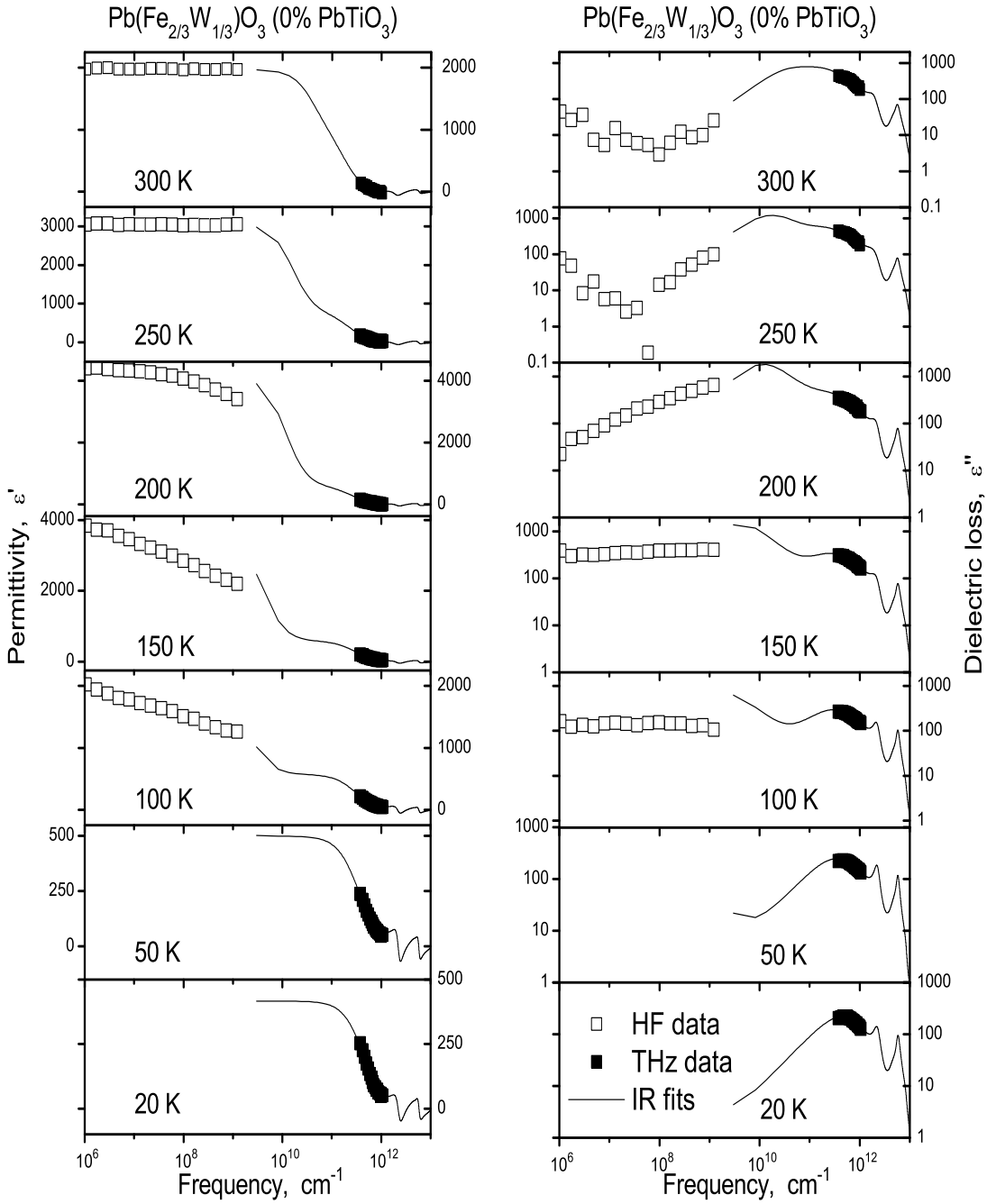

Figure 4.11 Low-temperature complex dielectric spectra of PFW obtained from the fit of IR and THz experimental data together with HF and THz experimental dielectric spectra.

4.4 Experimental Data of PFW-25% PT

In Figure 4.12 we present the temperature dependence of the permittivity, ε', and dielectric loss, ε'', obtained from the HF dielectric experiment at selected frequencies.

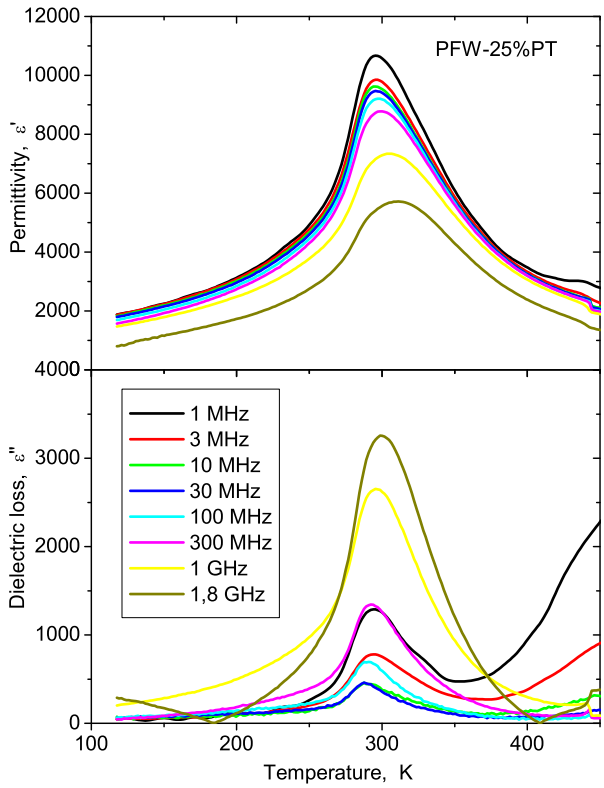

Figure 4.12 Temperature dependencies of PFW-25% PT at various frequencies of permittivity and dielectric loss in high-frequency range, where temperature independent T_m ($\sim$ 300 K) and conductivity (high temperatures) is observed.

There is a remarkable frequency dispersion in the whole measured temperature range across the whole measured FR. It can be seen that the peak of the permittivity is broad and the temperature of the permittivity maxima, T_m, does not move significantly with a changing frequency. Just a gentle shift towards higher temperatures with the increasing frequency is observed. We can say that the T_m (or T_c) is several Kelvin below 300 K in the explored FR. The permittivity

decreases with the increasing frequency, while the dielectric loss increases with the increasing frequency. This is a signature of the diffuse PhT (see Section 2.7) with relaxation frequency close to our spectral range.

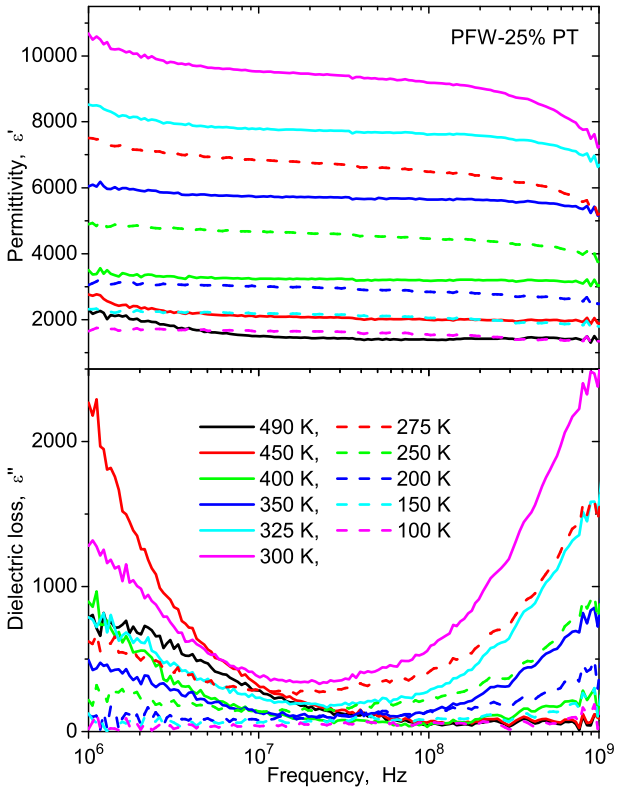

Figure 4.13 Frequency dependencies of complex dielectric response in HF range of PFW-25% PT.

In Figure 4.13 we present the permittivity and the dielectric loss spectra between 1 MHz and 1 GHz for selected temperatures. It can be seen that these data show great dispersion both at lower and higher frequencies in the whole temperature range. The dielectric loss arising at lower frequencies (< 10 GHz) is affected by conductivity (also discussed in Section 4.3 for previous sample), and the tails at high frequencies are affected by relaxator in MW range due to disorder in the lattice. Let us discuss the latter excitation. The high-frequency permittivity (above 100 MHz) firstly increases (dashed lines), its maximum appears at room-temperature, and then decreases (solid lines) on heating. It is a consequence of

slowing down of a relaxator in MW range. The dielectric spectra were fitted together with THz spectra (see Figure 4.15) by means of Cole-Cole formula (2.11) in the temperature range $150 - 420\,\mathrm{K}$. We came to a frequency dependence of the soft relaxation, which was fitted by the Cochran generalized formula,

$$\omega_r = A|T - T_c|, \tag{4.1}$$

where T_c is the Curie-Weiss (critical) temperature. Two critical temperatures were obtained, $T_{c1} = 290 \pm 10\,\mathrm{K}$ (with $C_{CW1} = -5.0 \times 10^7 \pm 0.1 \times 10^7\,\mathrm{K}$) and $T_{c2} = 370 \pm 10\,\mathrm{K}$ (with $C_{CW2} = 1.6 \times 10^8 \pm 0.1 \times 10^8\,\mathrm{K}$), see Figure 4.14. It gives evidence about the weak 1st order PhT (see Section 2.6). According to phase diagram (Figure 4.1), T_{c1} corresponds to the PhT temperature of PFW-25% PT.

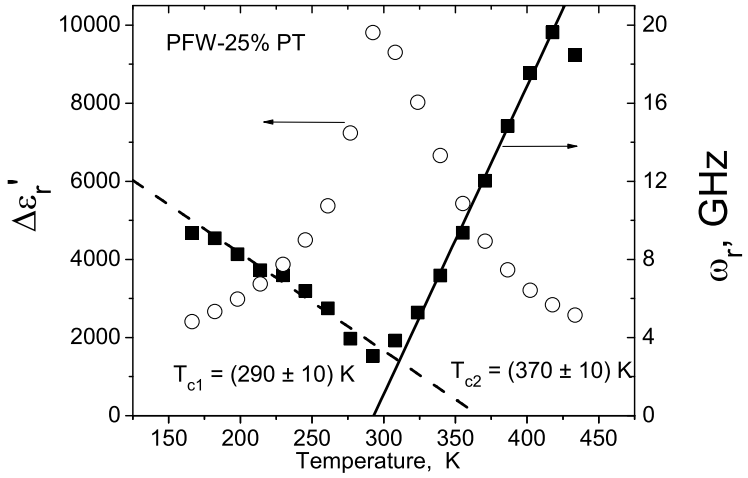

Figure 4.14 Cochran-like fits of relaxation frequency of the relaxator in PFW-25% PT in MW range.

It is true that the collected THz data cover only the temperature range $20 - 300\,\mathrm{K}$ (see Figure 4.15). It's been assumed that above 250 K the change of THz permittivity in FR $20 - 40\mathrm{cm}^{-1}$ is not dramatic, as can be seen in the depicted temperature range. But the dielectric loss seems to change remarkably. In the case of continuously growing dielectric loss at low frequencies, the connection between HF and THz spectra cannot be explained with one relaxator in MW range—there

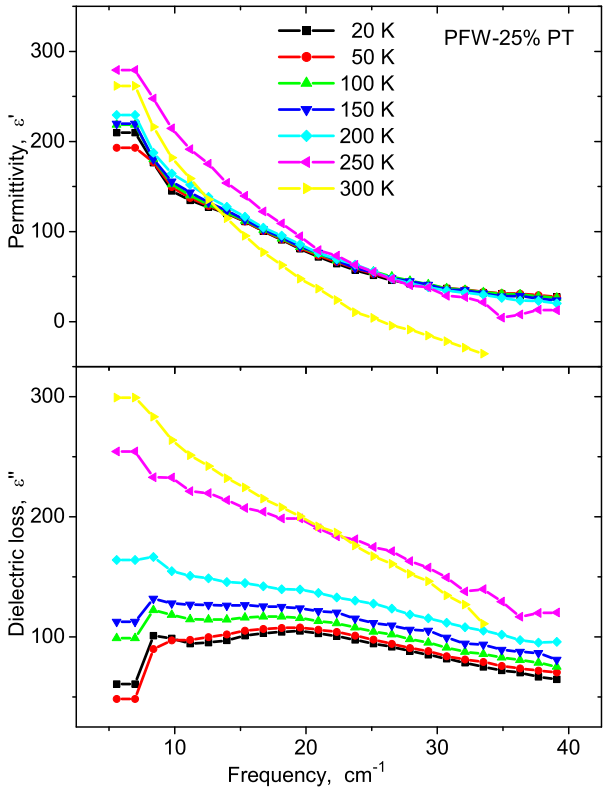

Figure 4.15 Experimental THz complex dielectric spectra of PFW-25% PT in the frequency range $0.3 - 1.3$ THz.

must be at least two relaxations, or some complicated distribution of relaxation times.

In Figure 4.16 the IR reflectivities for temperatures 20 K, 300 K and 600 K together with the fits are depicted. It is noteworthy that the reflectivity of the PFW-25% PT samples slightly grows with the increasing temperature, which is rather unusual. The components of complex permittivity are depicted in Figure 4.17.

Simple overdamped oscillator (3.6) was used to fit the LF IR reflectivity together with the THz data. Its contribution to permittivity, $\Delta\varepsilon'$, were taken from HF dielectric measurements.

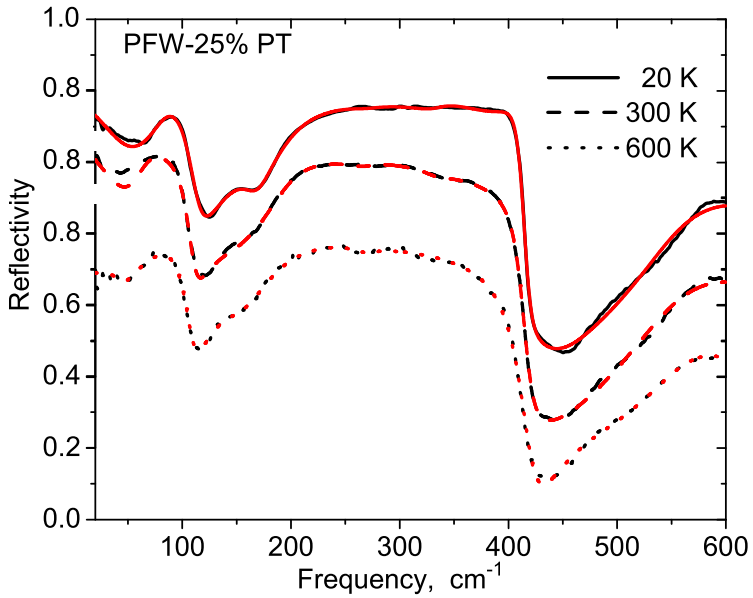

Figure 4.16 Measured (black line) and calculated (red line) IR reflectivity of PFW-25% PT ceramics at selected temperatures 20 K, 300 K and 600 K.

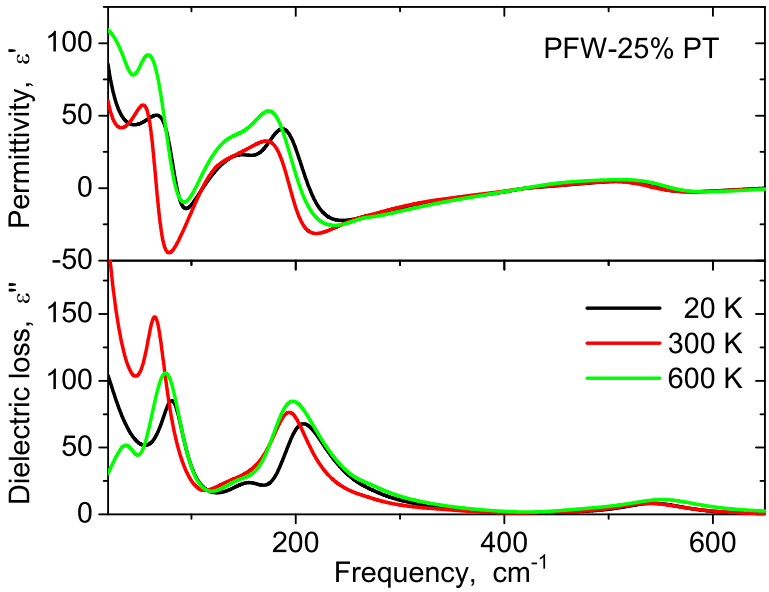

Figure 4.17 Calculated permittivity and dielectric loss spectra of PFW-25% PT.

In Figure 4.18 we present the TO frequencies of phonons obtained from the fits of the IR spectra. The anomaly of TO2 frequency near 300 K shows that the PhT is slightly driven by optic phonon softening, but it follows from Figure 4.14 that the whole dielectric dispersion near T_c is caused by soft MW relaxation.

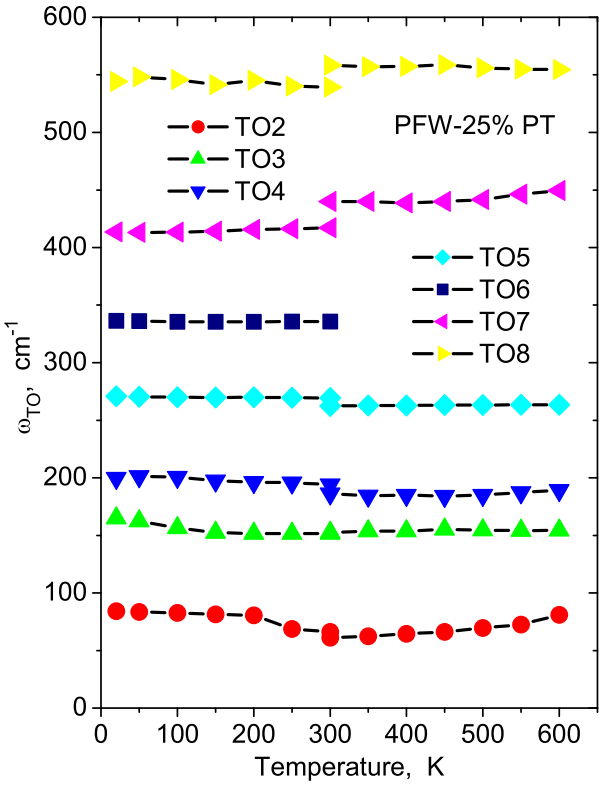

Figure 4.18 Temperature dependencies of transverse optic phonon frequencies in PFW-25% PT.

The extension of the fits into the MW FR can be seen in Figure 4.19 where HF dielectric, THz and IR data are shown. In spite of using classical damped (overdamped) oscillator as the relaxation in MW range pretty good correlation between HF, THz and IR spectra were achieved.

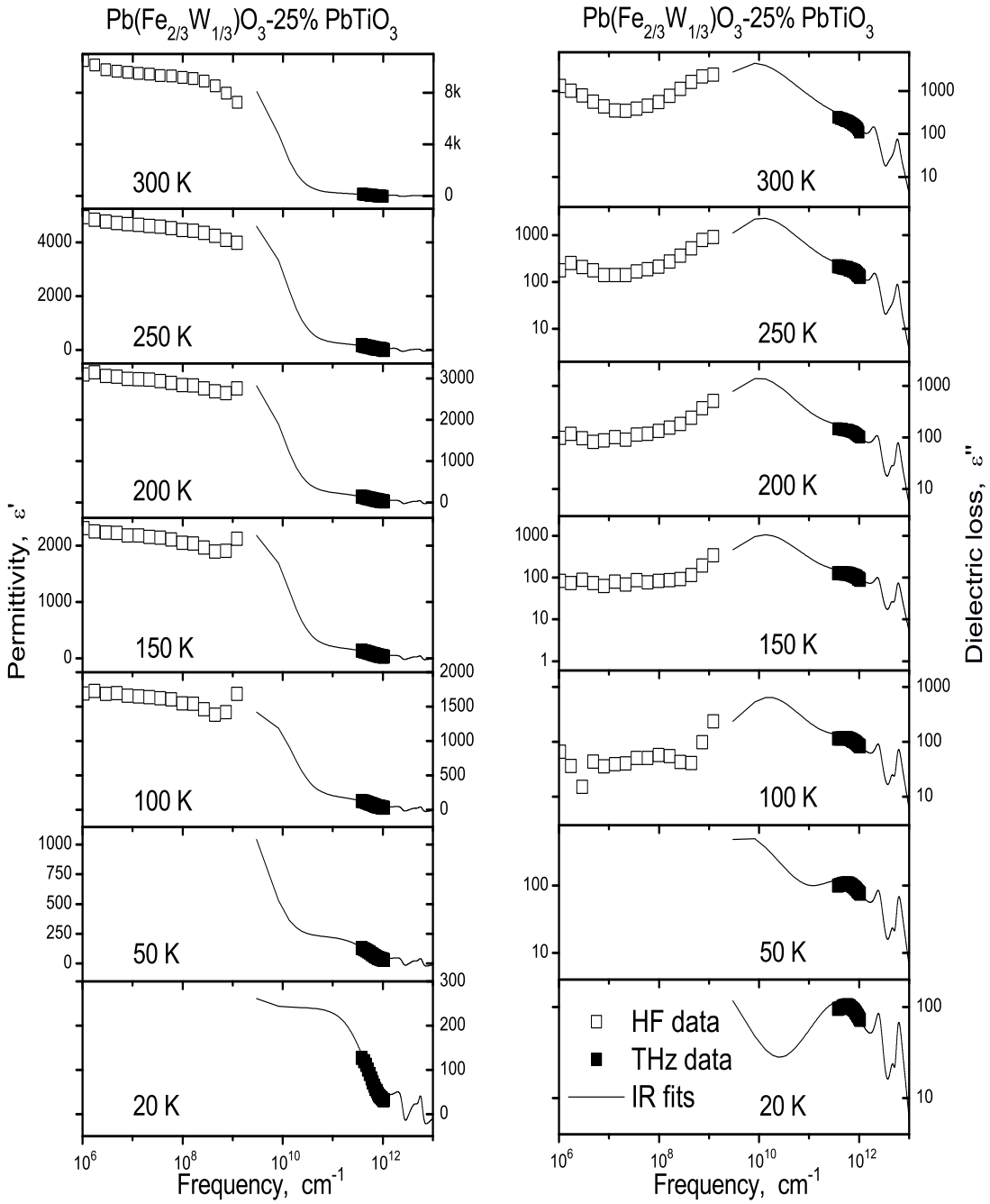

Figure 4.19 Low-temperature complex dielectric spectra of PFW-25% PT obtained from the fit of IR and THz experimental data together with HF and THz experimental dielectric spectra.

4.5 Experimental Data of PFW-37% PT

In Figure 4.20 we present the temperature dependencies of the permittivity, ε', and dielectric loss, ε'', obtained from the HF dielectric experiment at selected frequencies. There is no frequency dispersion in permittivity dependence in the investigated temperature and frequency range. The peak of the non-dispersive permittivity is broad, and the temperature of the permittivity maximum, $T_{\mathrm{m}} \neq T_{\mathrm{m}}(f)$, takes place at about 340 K, corresponding to the ferro- to paraelectric PhT. It has a typical shape of the normal FE PhT (see Section 2.7). At the same time the dielectric loss peak becomes higher with the increasing frequency. In comparison with PFW (Figure 4.2) and PFW-25% PT (Figure 4.12), no considerable conductivity appears below 450 K.

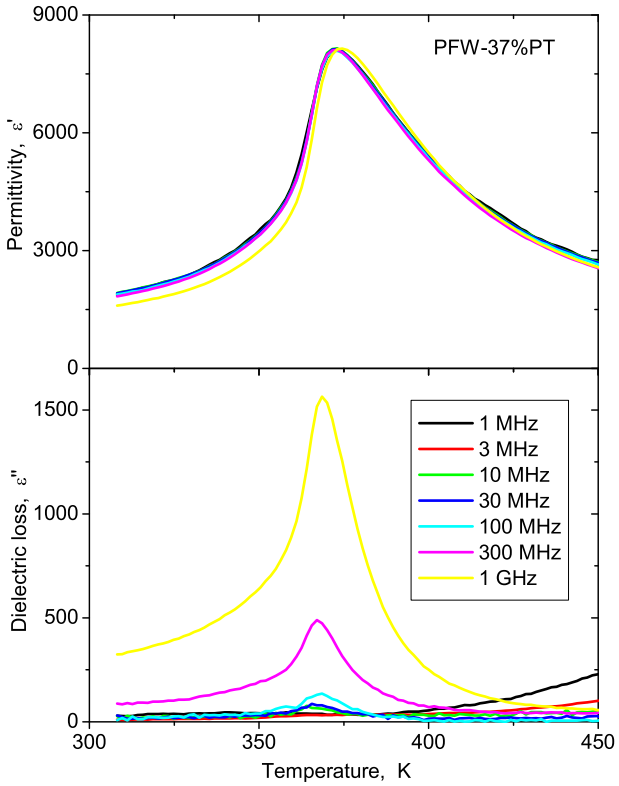

Figure 4.20 Temperature dependencies of permittivity and dielectric loss in PFW-37% PT.

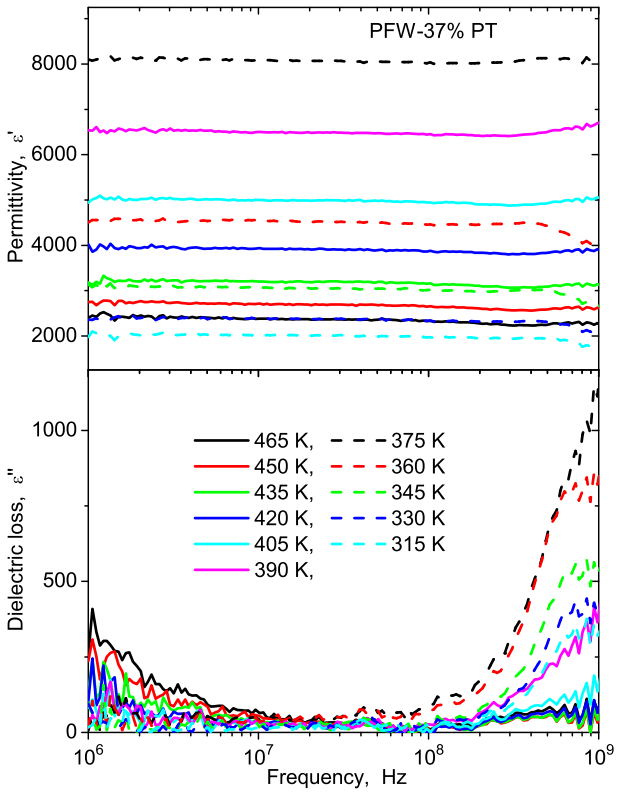

Figure 4.21 Frequency dependence of high-frequency data of PFW-37% PT, on the right the relaxation, on the left conductivity appears.

In Figure 4.21 we present the experimental permittivity and the dielectric loss spectra for selected temperatures. The small dispersion at lower frequencies in ε'' spectra (below 10 MHz) is assigned to conductivity, but this effect has practically negligible contribution to permittivity, ε'.

A high-frequency dielectric loss dispersion is assumed as a tail of a relaxator with the relaxation frequency above 10 GHz. This relaxation frequency firstly decreases with decreasing temperature and then increases as the temperature goes below T_c, sensible from frequency dependencies. We tried to fit the HF data together with THz data (Figure 4.22). However, the Cole-Cole fit with one relaxator was not successful. Two relaxations were needed but in this case the results of the fits were ambiguous due to the lack of data between 1 and 100 GHz, therefore these results are not presented here.

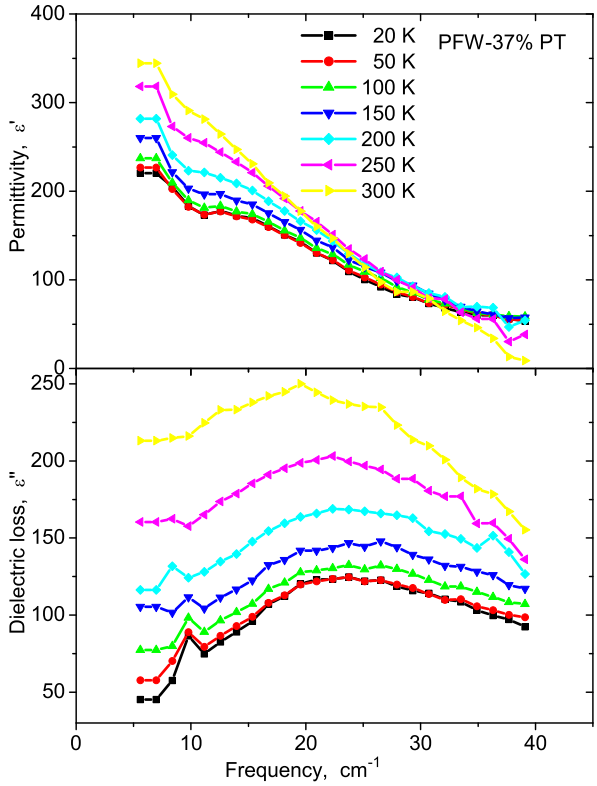

Figure 4.22 Experimental THz complex dielectric spectra of PFW-37% PT in the frequency range $0.3 - 1.3$ THz.

In the THz data a narrow and weak relaxation appears around $20 - 30\,\mathrm{cm}^{-1}$, which was fitted by means of overdamped oscillator model.

The experimental data and fitted curves of reflectivities and the components of complex permittivity are depicted for temperatures 20 K, 300 K and 550 K in Figure 4.23 and 4.24, respectively.

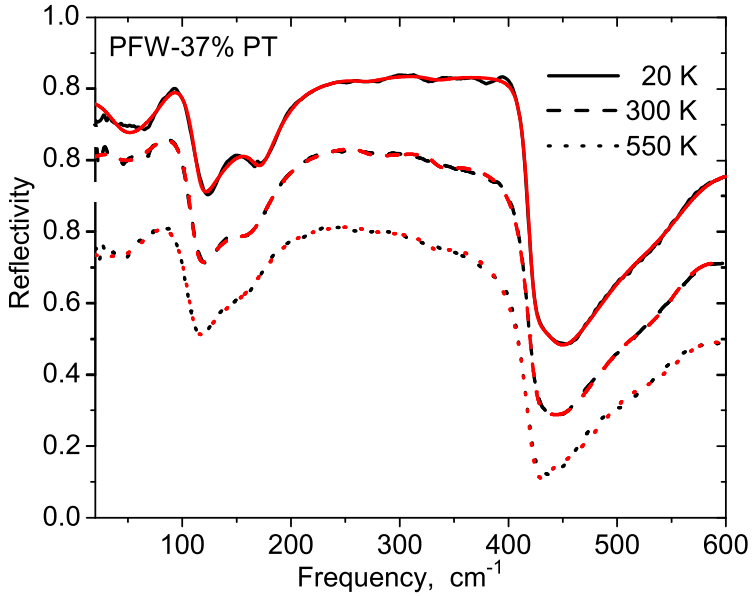

Figure 4.23 Measured (black line) and calculated (red line) reflectivity of PFW-37% PT ceramics for selected temperatures.

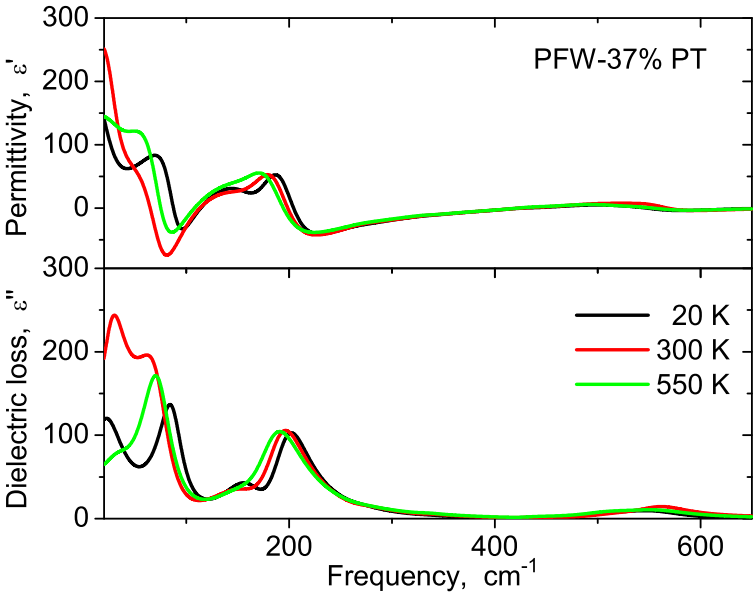

Figure 4.24 Permittivity and dielectric loss spectra calculated from the fits of IR reflectivity spectra.

In Figure 4.25 we present the temperature dependencies of the TO phonon frequencies. An anomaly of the TO2 mode near 400 K shows that the respective phonon feels the structural PhT, but it is clear that the dielectric anomaly near T_c in Figure 4.20 is caused by a soft MW relaxation, like in previous PFW and PFW-25% PT samples.

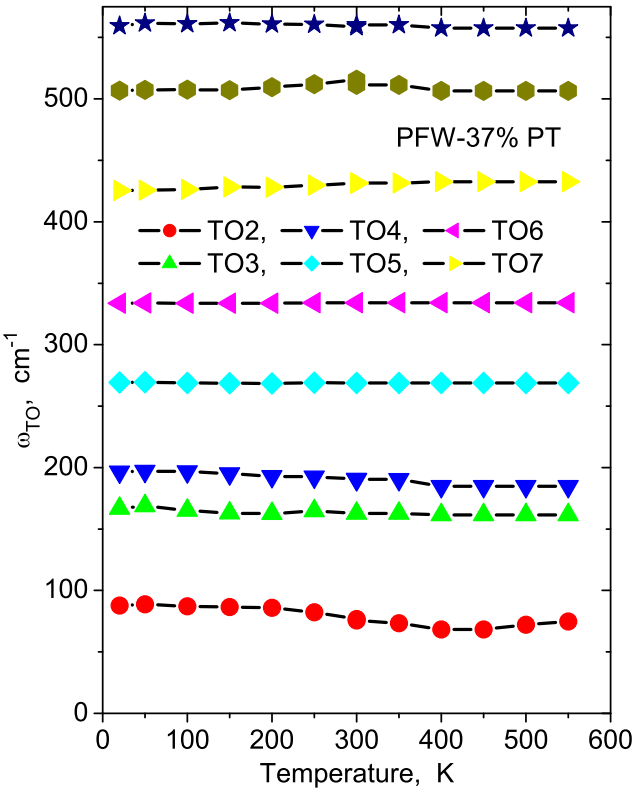

Figure 4.25 Transverse optic phonon frequencies in IR range of PFW-37% PT were obtained by means of four-parameter generalized oscillator model (3.7).

The extension of the IR fits into the MW FR can be seen in Figure 4.26 where HF dielectric, THz and IR data are shown. In spite of using classical damped oscillator in MW range (instead of relaxator), pretty good agreement between experimental data and theoretical curves was achieved.

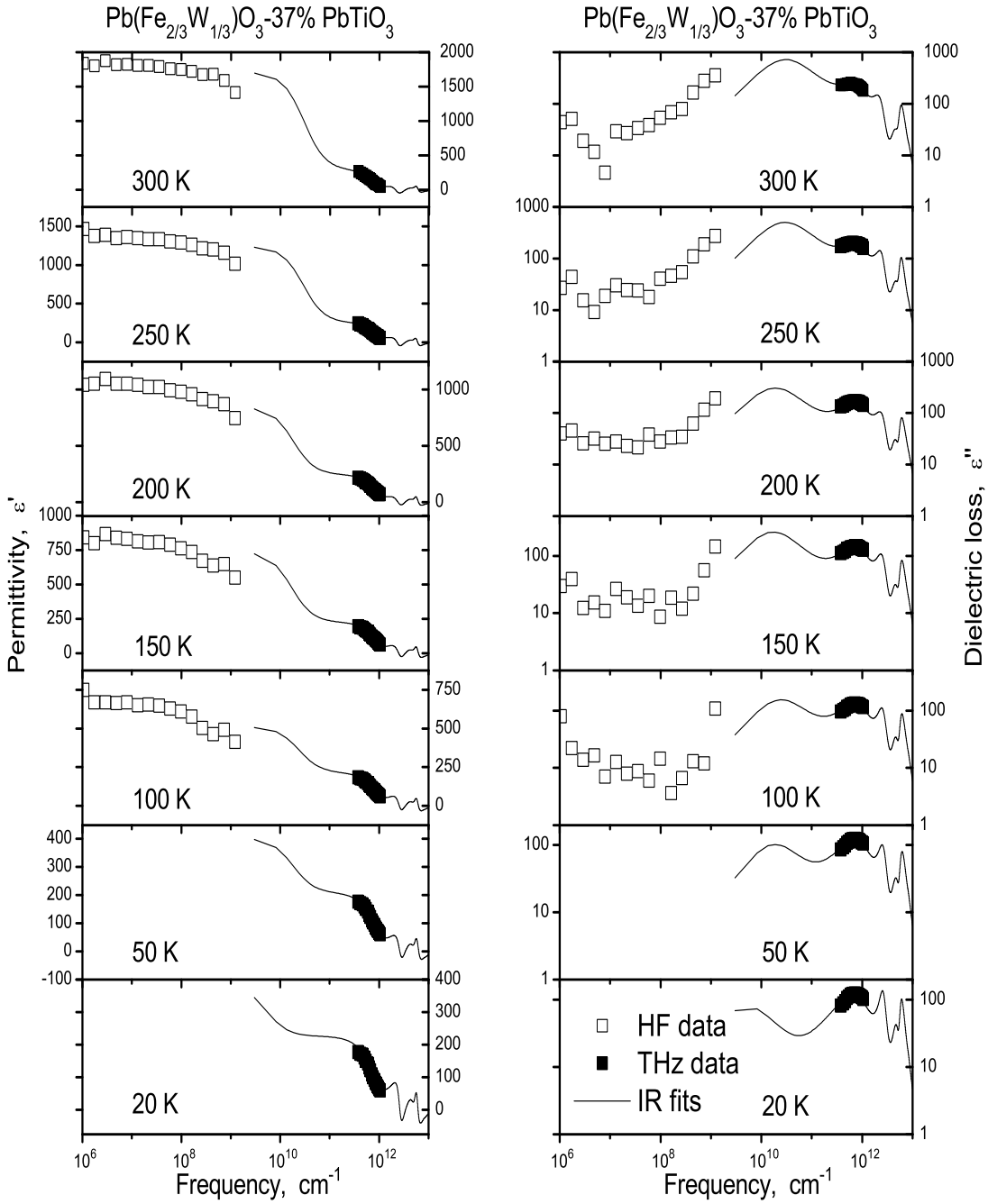

Figure 4.26 Low-temperature complex dielectric spectra of PFW-37% PT obtained from the fit of IR and THz experimental data together with HF and THz experimental dielectric spectra.

Chapter 5

Summary and Conclusions

This thesis reports on complex dielectric response of pure relaxor ferroelectrics PFW and two solid solutions of $(1-x)$PFW-(x)PT ($x = 0.25$ and 0.37) to understand the dynamics of PhTs in these materials. The complex dielectric function at frequencies between 1 MHz and 100 THz (except the MW range, from 2 GHz to 300 GHz) under isothermal conditions at temperatures from 20 K to 550 K was measured by means of HF dielectric and FT-IR spectroscopy and TDTS.

The author mastered the work with various experimental techniques, such as FT-IR (spectrometer Bruker IFS-113v) and HF dielectric spectroscopy, TDTS, including helium- and nitrogen-cooling techniques, heating to high-temperatures and manipulation with sensitive solid samples. Also various fitting techniques, such as application of several oscillator models to the reflectivity spectra, fitting the complex dielectric function with the Cole-Cole model, were mastered by the author.

The studies performed make it possible to draw the following conclusions.

The experimental data of all three samples revealed dielectric relaxation below the polar phonon frequencies. The relaxation frequency of the relaxation spreads between 2 GHz and 300 GHz in the whole measured temperature region. The dielectric strength of this relaxation is nearly two orders of magnitude larger then the sum of dielectric strengths of polar optic phonons, therefore, the contribution of the optic phonons to the permittivity is negligible.

The slowing down of the relaxation and its broadening on cooling is responsible for the relaxor behavior (diffuse dielectric anomaly near T_m) in pure PFW. The relaxation is due to to polar cluster dynamics. The freezing temperature of pure PFW was assigned to 170 K. The slowing down of the relaxation to T_c and its hardening below this temperature on further cooling was observed in PFW-25% PT. This confirms diffuse and order-disorder character of the PhT in this material. PFW-37% PT exhibits normal ferroelectric phase transition. The relaxation frequency lies at higher frequencies, therefore, it was not possible to evaluate it in details, but it probably exhibits a behavior qualitatively similar to that observed in PFW-25% PT.

No phonon softening was observed in these solid solutions. This is compatible with the relaxor nature of the ferroelectricity in the PFW ceramics and with order-disorder character of PhTs in all the investigated ceramics.

Future research in this field will be focused on investigation by means of MW coaxial techniques and on research into ferromagnetic properties.

Bibliography

[Ahn 04] C. H. Ahn, K. M. Rabe & J.-M. Triscone. *Ferroelectricity at the Nanoscale: Local Polarization in Oxide Thin Films and Heterostructures*. Science, vol. 303, pages 488–91, January 2004.

[Anderson 60] P. Anderson. Fizika dielektrikov. Akad. Nauk USSR, Moscow, 1960.

[Anselm 67] A. I. Anselm. Úvod do teorie polovodičů. Academia, nakl. ČSAV, Praha, 1st edition, 1967.

[Bell 72] R. J. Bell. Introductory Fourier transform spectroscopy. Academic Press, New York, 1972.

[Berreman 68] Dwight Berreman & F. C. Unterwald. *Adjusting Poles and Zeros of Dielectric Dispersion to Fit Reststrahlen of $PrCl_3$ and $LaCl_3$*. Phys. Rev., vol. 174, no. 3, pages 791–9, October 1968.

[Bovtun 04] Viktor Bovtun, Stanislav Kamba, Alexej Pashkin, Maxim Savinov, Polina Samoukhina, Jan Petzelt, Igor P. Bykov & Maya D. Glinchuk. *Central-Peak Components and Polar Soft Mode in Relaxor $PbMg_{1/3}Nb_{2/3}O_3$ Crystals*. Ferroelectrics, vol. 298, pages 23–30, 2004.

[Bovtun 05] Viktor Bovtun, 2005. personal oral consultation.

[Buixaderas 01] Elena Lopéz Buixaderas. *Spectroscopic Investigation of Lattice Dynamics and its Disorder in Ferroelectric and Related Materials*.

PhD thesis, Departmento de Física Aplicada I,Universidad del País Vasco, Bilbao, 2001.

[Cochran 59] W. Cochran. *Crystal Stability and the Theory of Ferroelectricity*. Phys. Rev. Lett., vol. 3, page 412, 1959.

[Courtens 84] Eric Courtens. *Vogel-Fulcher Scaling of the Susceptibility in a Mixed-Crystal Proton Glass*. Phys. Rev. Lett., vol. 52, pages 69–72, January 1984.

[Courtens 86] Eric Courtens. *Scaling Dielectric Data on $Rb_{1-x}(NH_4)_xH_2PO_4$ Structural Glasses and their Deuterated Isomorphs*. Phys. Rev. B, vol. 33, no. 4, pages 2975–8, February 1986.

[Cross 94] L. Eric Cross. *Relaxor Ferroelectrics: An Overview*. Ferroelectrics, vol. 151, pages 305–20, 1994.

[Daniel 67] Vera V. Daniel. Dielectric relaxation. Academic Press, London and New York, 1967.

[Dougherty 94] Thomas P. Dougherty, Gary P. Wiederrecht, Keith A. Nelson, Mark H. Garrett, Hans P. Jenssen & Cardinal Warde. *Femtosecond Time-Resolved Spectroscopy of Soft Modes in Structural Phase Transitions of Perovskites*. Phys. Rev. B, vol. 50, no. 13, pages 8996–9019, 1994.

[Feng 02] L. Feng & Z.-G. Ye. *Phase Diagram and Phase Transitions in the Relaxor Ferroelectric $Pb(Fe_{2/3}W_{1/3})O_3$-$PbTiO_3$ System*. J. of Solid State Chemistry, vol. 163, pages 484–90, 2002.

[Fröhlich 49] H. Fröhlich. Theory of dielectrics: Dielectric constant and dielectris loss. Clarendon Press, Oxford, 1st edition, 1949.

[Grigas 96] J. Grigas. Microwave dielectric spectroscopy of ferroelectrics and related materials. Gordon and Breach, Amsterdam, 1996.

[Hench 90] Larry L. Hench & Jon K. West. Principles of electronic ceramics. John Wiley & Sons, Inc., 1990.

[Jonscher 83] Andrew K. Jonscher. Dielectric relaxation in solids. Chelsea Dielectrics Press Limited, London, 1983.

[Kamba 02] Stanislav Kamba, Susan Trolier-McKinstry, Alexej Paschkin, Viktor Bovtun & Jan Petzelt. *Anomaluos Broad Dielectric Relaxation in $Bi_{2/3}ZnNb_{2/3}O_7$ Pyrochlore*. Phys. Rev. B, vol. 66, page 054106, 2002.

[Kittel 85] Charles Kittel. Úvod do fyziky pevných látek. Academia, nakl. ČSAV, Praha, 1st edition, 1985. orig.: Introduction to Solid State Physics (John Wiley and Sons, Inc.), 5th ed.

[Kužel 00] Petr Kužel & Jan Petzelt. *Time-Resolved Terahertz Transmission Spectroscopy of Dielectrics*. Ferroelectrics, vol. 239, pages 949–56, 2000.

[Kužel 04] Peter Kužel. *THz Spectroscopy*. http://www.fzu.cz/departments/dielectrics/groups/optics.html (http://tinyurl.com/3wqq4), 2004.

[Landau 37] L. D. Landau. Phys. Z. Sowjun, vol. 11, no. 26, page 545, 1937.

[Landau 64] L. D. Landau & E. M. Lifsic. Statisticeskaja fizika. Nauka, Moskva, 1964.

[Lines 77] M. E. Lines & A. M. Glass. Principles and application of ferroelectrics and related materials. Claredon Press, Oxford, 1977.

[Mitoseriu 02a] Liliana Mitoseriu, Paula M. Vilarinho & João L. Baptista. *Phase Coexistence in $Pb(Fe_{2/3}W_{1/3})O_3$-$PbTiO_3$ Solid Solutions*. Appl. Phys. Lett., vol. 80, no. 23, pages 4422–4, June 2002.

[Mitoseriu 02b] Liliana Mitoseriu, Paula M. Vilarinho & João L. Baptista. *Properties of $Pb(Fe_{2/3}W_{1/3})O_3$-$PbTiO_3$ System in the Range of Morphotropic Phase Boundary*. Jpn. J. Appl. Phys., vol. 41, pages 7015–20, November 2002.

[Mitoseriu 02c] Liliana Mitoseriu, Paula M. Vilarinho, Massimi Viviani & João L. Baptista. *Structural Study of $Pb(Fe_{2/3}W_{1/3})O_3$-$PbTiO_3$ System*. Material Letters, vol. 57, pages 609–14, 2002.

[Mitoseriu 03a] Liliana Mitoseriu, Daniele Marré, Antonio Sergio Siri & Paolo Nanni. *Magnetic Properties of $Pb(Fe_{2/3}W_{1/3})O_3$-$PbTiO_3$ Solid Solutions*. Appl. Phys. Lett., vol. 83, no. 26, pages 5509–11, December 2003.

[Mitoseriu 03b] Liliana Mitoseriu, Alexandru Stancu & Cristina E. Fedor. *Analysis of the Dielectric Constant Data of Relaxors within a Landau-Type Theory*. J. Opt. Adv. Mat., vol. 5, no. 3, pages 787–90, September 2003.

[Mitoseriu 03c] Liliana Mitoseriu, Alexandru Stancu, Cristina E. Fedor & Paula M. Vilarinho. *Analysis of the Composition-Induced Transition from Relaxor to Ferroelectric State in $Pb(Fe_{2/3}W_{1/3})O_3$-$PbTiO_3$ Solid Solutions*. J. Appl. Phys., vol. 94, no. 3, pages 1918–25, August 2003.

[Mitoseriu 04] Liliana Mitoseriu, Maria M. Carnasciali, Paolo Piaggio & Paolo Nanni. *Raman Investigation of the Composition and Temperature-Induced Phase Transition in $(1-x)Pb(Fe_{2/3}W_{1/3})O_3$-$xPbTiO_3$ Ceramics*. J. Appl. Phys., vol. 96, no. 8, pages 4378–85, October 2004.

[Ostapchuk 04] Tetyana Ostapchuk. *Far Infrared Spectroscopy of Ferroelectric and Related Thin Films and Ceramics*. PhD thesis, Faculty of Mathematics and Physics, Charles University in Prague, 2004.

[Park 97] SeungEek Park & Thomas S. Shrout. *Ultrahigh Strain and Piezoelectric Behavior in Relaxor Based Ferroelectric Piezoelectric Single Crystals*. J. Appl. Phys., vol. 82, pages 1804–11, 1997.

[Pashkin 04] Alexej Pashkin. *Terahertz Spectroscopy of Ferroelectrics and Related Materials*. PhD thesis, Faculty of Mathematics and Physics, Charles University in Prague, 2004.

[Petzelt 76] Jan Petzelt & Jan Fousek. *Strukturní fázové přechody v krystalech*. Československ. čas. pro fyziku, vol. 26, no. 4, pages 337–448, 1976.

[Porokhonskyy 04] Viktor Porokhonskyy. *Dielectric Spectroscopy of Some High-Permittivity Ceramics with Structural Disorder*. PhD thesis, Faculty of Mathematics and Physics, Charles University in Prague, 2004.

[Samara 01] G. A. Samara. Ferroelectricity revisited—Advances in materials and physics, in Solid State Physics, volume 56. Academic Press, San Diego, 2001.

[Samara 03] George A. Samara. *The Relaxational Properties of Compositionally Disordered ABO_3 Perovskites*. J. Phys.: Condens. Matter, vol. 15, pages R367–R411, 2003.

[Schevchuk 97] Y. A. Schevchuk, S. K. Korchagina, V. V. Gagulin & V. V. Bogatko. *Synthesis and Investigation of Solid Solutions Based on Relaxor Ferroelectric-Antiferromagnetic $Pb(Fe_{2/3}W_{1/3})0_3$*. Ferroelectrics, vol. 199, pages 223–30, 1997.

[Schevchuk 99] Y. A. Schevchuk, S. K. Korchagina & V. V. Gagulin. *Relaxation in Ferroelectric Solid Solutions of the System $Pb(Fe_{2/3}W_{1/3})O_3$-$PbTiO_3$ over the Microwave Range*. Ferroelectrics, vol. 235, pages 269–74, 1999.

[Szwagierczak 04] D. Szwagierczak & J. Kulawik. *Thick Film Capacitors with Relaxor Dielectrics*. J. Eu. Ceram. Soc., vol. 24, pages 1979–85, 2004.

[Tagantsev 94] A. K. Tagantsev. *Vogel-Fulcher Relationship for the Dielectric Permittivity of Relaxor Ferroelectrics*. Phys. Rev. Lett., vol. 72, pages 1100–3, 1994.

[Uchino 94] Kenji Uchino. *Relaxor Ferroelectrics Devices*. Ferroelectrics, vol. 151, pages 321–30, 1994.

[Vilarinho 00] Paula M. Vilarinho, Liqin Zhou, Manfred Pöckl, Nelson Marques & João L. Baptista. *Dielectric Properties of $Pb(Fe_{2/3}W_{1/3})O_3$-$PbTiO_3$ Solid-Solution Ceramics*. J. Am. Ceram. Soc., vol. 83, page 1149, 2000.

[Vilarinho 02] P. M. Vilarinho, L. Zhou, L. Mitoseriu, E. Finocchio, M. R. Soares & J. L. Baptista. *Morphotropic Phase Boundary In $Pb(Fe_{2/3}W_{1/3})O_3$-$PbTiO_3$ System*. Ferroelectrics, vol. 270, pages 253–8, 2002.

[Vugmeister 97] B. E. Vugmeister & H. Rabitz. *A Phenomenology of Relaxor Ferroelectrics*. Ferroelectrics, vol. 201, pages 33–42, 1997.

[Waser 03] Rainer Waser, editeur. Nanoelectronics and information technology. Wiley-VCH Verlag GmbH & Co. KGaA, Weinheim, 2003.

[Ye 98a] Z.-G. Ye. *Relaxor Ferroelectric Complex Perovskites: Structure, Properties and Phase Transitions*. Key Engineering Materials, vol. 155–156, pages 81–122, 1998.

[Ye 98b] Z.-G. Ye, K. Toda, M. Sato, E. Kita & H. Schmid. *Synthesis, Structure and Properties od the Magnetic Relaxor Ferroelectric $Pb(Fe_{2/3}W_{1/3})O_3$ [PFW]*. J. Kor. Phys. Soc., vol. 32, pages S1028–S1031, February 1998.

List of Symbols

α	parameter of the distribution of relaxation times
γ_{LO}	longitudinal damping, Hz
γ_{TO}	transverse damping, Hz
$\Delta\varepsilon'$	contribution to permittivity
ε'	real part of complex permittivity
ε''	imaginary part of complex permittivity
$\varepsilon'(0)$	static permittivity
ε^*	complex permittivity
ε_0	permittivity of the free space, $10^7/4\pi c_0^2\,\mathrm{F{\cdot}m^{-1}} = 8.854 \times 10^{-12}\,\mathrm{F{\cdot}m^{-1}}$
ε'_∞	high-frequency permittivity
ε_{r}	relative permittivity
η	transition parameter
κ	imaginary part of complex refractive index
λ	wavelength, m
ν	wavenumber, cm^{-1}
ω	frequency, Hz
ω_{LO}	longitudinal frequency, Hz
ω_{m}	frequency of a maximum (in the spectra), Hz
ω_{r}	relaxation frequency of relaxator, Hz
ω_{TO}	transverse frequency, Hz
χ	dielectric susceptibility

C_{CW}	Curie-Weiss constant, $F \cdot K \cdot m^{-1}$
$\mathbf{D}$	dielectric displacement, $C \cdot m^{-2}$
$\mathbf{E}$	electric field, $V \cdot m$
f	frequency, Hz
$g(\tau)$	distribution of Debye relaxation times
k	Boltzmann constant, $1.38 \times 10^{-23}\,J \cdot K^{-1}$
N	count or number
n	real part of complex refractive index
n^*	complex refractive index
$\mathbf{P}$	electrical polarization, $C \cdot m^{-2}$
$\mathbf{P}_s$	spontaneous polarization, $C \cdot m^{-2}$
R	reflectivity
T	temperature, K
T_c	Curie-Weiss (critical) temperature, K
T_d	Burns temperature, K
T_m	temperature of permittivity maximum, K
T_{VF}	Vogel-Fulcher temperature, K

List of Abbreviations

EM	Electromagnetic
FE	Ferroelectric
FIR	Far-Infrared
FR	Frequency Range
FT-IR	Fourier Transform Infrared
HF	High-Frequency
INS	Inelastic Neutron Scattering
IR	Infrared
LF	Low-Frequency
LO	Longitudinal Optical
LST	Lyddane-Sachs-Teller
MIR	Middle-Infrared
MPB	Morphotropic Phase Boundary
MW	Microwave
PE	Paraelectric
PFW	$Pb(Fe_{2/3}W_{1/3})O_3$
PFW-PT	$Pb(Fe_{2/3}W_{1/3})O_3$-$PbTiO_3$
PhT	Phase Transition
PMN	$Pb(Mg_{1/3}Nb_{2/3})O_3$
PT	$PbTiO_3$
PZN	$Pb(Zn_{1/3}Nb_{2/3})O_3$
SM	Soft Mode
TDTS	Time-Domain Terahertz Spectroscopy
TO	Transverse Optical